Black and brown carbon over central Amazonia: Long-term aerosol measurements at the ATTO site

Jorge Saturno[1], Bruna A. Holanda[1], Christopher Pöhlker[1], Florian Ditas[1], Qiaoqiao Wang[1,2], Daniel Moran-Zuloaga[1], Joel Brito[3,4], Samara Carbone[3,5], Yafang Cheng[1], Xuguang Chi[6], Jeannine Ditas[1,2], Thorsten Hoffmann[7], Isabella Hrabe de Angelis[1], Tobias Könemann[1], Jošt V. Lavrič[8], Nan Ma[1,2], Jing Ming[1], Hauke Paulsen[9], Mira L. Pöhlker[1], Luciana V. Rizzo[10], Patrick Schlag[3], Hang Su[1], David Walter[1], Stefan Wolff[1], Yuxuan Zhang[1], Paulo Artaxo[3], Ulrich Pöschl[1], and Meinrat O. Andreae[1,11]

[1]Biogeochemistry & Multiphase Chemistry Departments, Max Planck Institute for Chemistry, P. O. Box 3060, 55020 Mainz, Germany.
[2]Jinan University Institute for Environmental and Climate Research, Guangzhou, China.
[3]Department of Applied Physics, Institute of Physics, University of São Paulo (USP), Rua do Matão, Travessa R, 187, CEP 05508-900, São Paulo, SP, Brazil.
[4]Laboratory for Meteorological Physics, Université Clermont Auvergne, Clermont-Ferrand, France.
[5]Institute of Agrarian Sciences, Federal University of Uberlândia, Uberlândia, Minas Gerais, Brazil.
[6]Institute for Climate and Global Change Research & School of Atmospheric Sciences, Nanjing University, Nanjing, 210093, China.
[7]Department of Chemistry, Johannes Gutenberg University, Mainz, Germany.
[8]Biogeochemical Systems & Biogeochemical Processes Departments, Max Planck Institute for Biogeochemistry, 07701 Jena, Germany.
[9]Institute of General Botany, Johannes Gutenberg University, Mainz, Germany.
[10]Departamento de Ciencias Ambientais, Universidade Federal de Sao Paulo, Diadema, SP, Brasil.
[11]Scripps Institution of Oceanography, University of California San Diego, La Jolla, CA 92098, USA.

Correspondence to: Jorge Saturno (j.saturno@mpic.de) and Christopher Pöhlker (c.pohlker@mpic.de)

Abstract. The Amazon rain forest is a sensitive ecosystem experiencing the combined pressures of progressing deforestation and climate change. Its atmospheric conditions oscillate between biogenic and biomass burning (BB) dominated states. The Amazon further represents one of the few remaining continental places where the atmosphere approaches pristine conditions during occasional wet season episodes. The Amazon Tall Tower Observatory (ATTO) has been established in central Amazonia to investigate the complex interactions between the rain forest ecosystem and the atmosphere. Physical and chemical aerosol properties have been analyzed continuously since 2012. This paper provides an

in-depth analysis of the aerosol's optical properties at ATTO based on data from 2012 to 2017. The following key results have been obtained:

- The aerosol scattering and absorption coefficients at 637 nm, $\sigma_{sp\ 637}$ and $\sigma_{ap\ 637}$, show a pronounced seasonality with lowest values in the clean wet season (mean ± SD: $\sigma_{sp\ 637}$ = 7.5 ± 9.3 Mm^{-1}; $\sigma_{ap\ 637}$ = 0.68 ± 0.91 Mm^{-1}) and highest values in the BB-polluted dry season ($\sigma_{sp\ 637}$ = 33 ± 25 Mm^{-1}; $\sigma_{ap\ 637}$ = 4.0 ± 2.2 Mm^{-1}). The single scattering albedo at 637 nm, ω_0, is lowest during the dry season (ω_0 = 0.87 ± 0.03) and highest during the wet season (ω_0 = 0.93 ± 0.04).
- The retrieved BC mass absorption cross sections, α_{abs}, are substantially higher than values widely used in the literature (i.e., 6.6 $m^2\ g^{-1}$ at 637 nm wavelength), likely related to thick organic or inorganic coatings on the BC cores. Wet season values of α_{abs} = 11.4 ± 1.2 $m^2\ g^{-1}$ (637 nm) and dry season values of α_{abs} = 12.3 ± 1.3 $m^2\ g^{-1}$ (637 nm) were obtained.
- The BB aerosol during the dry season is a mixture of rather fresh smoke from local fires, somewhat aged smoke from regional fires, and strongly aged smoke from African fires. The African influence appears to be substantial with its maximum from August to October. The interplay of African vs. South American BB emissions determines the aerosol optical properties (e.g., the fractions of black vs. brown carbon, BC vs. BrC).
- By analyzing the diel cycles, it was found that particles from elevated aerosol-rich layers are mixed down to the canopy level in the early morning and particle number concentrations decrease towards the end of the day. Brown carbon absorption at 370 nm, $\sigma_{ap\ BrC\ 370}$, was found to decrease earlier in the day likely due to photo-oxidative processes.
- BC to CO enhancement ratios, ER_{BC}, reflect the variability of burnt fuels, combustion phases, and atmospheric removal processes. A wide range of ER_{BC} between 4 and 15 ng m^{-3} ppb^{-1} was observed with higher values during the dry season, corresponding to the lowest ω_0 levels (0.86 – 0.93).
- The influence of the 2009/10 and 2015/16 El Niño periods and the associated increased fire activity on aerosol optical properties was analysed by means of nine-year σ_{sp} and σ_{ap} time series (combination of ATTO and ZF2 data). Significant El Niño-related enhancements were observed: in

the dry season, $\sigma_{sp\ 637}$ increased from 24 ± 18 Mm^{-1} to 48 ± 33 Mm^{-1} and $\sigma_{ap\ 637}$ from 3.8 ± 2.8 Mm^{-1} to 5.3 ± 2.5 Mm^{-1}.

- The absorption Ångström exponent, $å_{abs}$, representing the aerosol absorption wavelength dependence was mostly < 1.0 with episodic increases upon smoke advection. A parameterization of $å_{abs}$ as a function of the BC to OA mass ratio for Amazonian aerosol ambient measurements is presented. The brown carbon (BrC) contribution to σ_{ap} at 370 nm was obtained by calculating the theoretical BC $å_{abs}$, resulting in BrC contributions of 17 - 29 % (25th and 75th percentiles) to $\sigma_{ap\ 370}$ for the entire measurement period. The BrC contribution increased to 27 - 47 % during fire events under El Niño-related drought conditions from September to November 2015.

The results presented here may serve as a basis to understand Amazonian atmospheric aerosols in terms of their interactions with solar radiation and the physical and chemical-aging processes that they undergo during transport. Additionally, the analyzed aerosol properties during the last two El Niño periods in 2009/10 and 2015/16 offer insights that could help to assess the climate change-related potential for forest-dieback feedbacks under warmer and drier conditions.

1 Introduction

Atmospheric aerosol particles affect the Earth's climate through different mechanisms. Direct mechanisms include the aerosol particle interactions with radiation by scattering and absorption. The balance between scattering and absorption can lead to warming or cooling of the atmosphere (IPCC, 2013). Moreover, indirect mechanisms, like aerosol-cloud interactions during cloud formation and cloud microphysical modifications, are accompanied by high uncertainties, especially due to the lack of knowledge on pre-industrial levels of cloud condensation nuclei (CCN) (Carslaw et al., 2013) and aerosol spatial distribution in the atmosphere (Andreae, 2007).

Continuous aerosol measurements at remote continental locations are crucial to understand atmospheric conditions prior to industrialization and reduce the uncertainties in climate models (Seinfeld et al., 2016). The Amazon Basin is one of the few continental areas in the world where the atmosphere

approximates pristine conditions during some periods of the year (Andreae et al., 2015; Pöhlker et al., 2017). However, anthropogenic pollution is rather persistent and, thus, reaches almost every place in the planet (Andreae, 2007; Chi et al., 2013; Hamilton et al., 2014). The Amazon rain forest has been impacted substantially by intensified agriculture and the associated deforestation, and infrastructural development in the last 50 years (Artaxo et al., 2013; Davidson et al., 2012). Given these circumstances, only when air masses travel over clean marine areas and rain-related scavenging is significant, the observations approach near-pristine to pristine levels (Andreae et al., 2012, 2015; Pöhlker et al., 2017).

Biogenic primary and secondary organic aerosol particles over the Amazon rain forest are ubiquitous throughout the year (Martin et al., 2010b). During the dry season (August – November), when fires are frequent in the forest and its peripheries, the background biogenic aerosol is overwhelmed by BB smoke (Andreae et al., 1988; Artaxo et al., 2002; Fuzzi et al., 2007; Guyon et al., 2003a; Roberts et al., 2003). Despite the rare occurrence of natural tropical forest fires (Cochrane, 2003; Nepstad et al., 2008), most of the fire episodes in the Amazon rain forest peripheries occur due to human activity, including land use change, brush clearing for agricultural activities, burning of agricultural waste (Andreae, 1991; Crutzen and Andreae, 1990), and cooperative burning of savannas by indigenous communities, which is done to prevent larger wildfires (Bilbao et al., 2010). Starting in August, the dry season is characterized by aerosol number concentrations of 1000 – 3000 cm^{-3} (Andreae et al., 2015). Another characteristic of the dry season is the occurrence of abundant black carbon (BC) in the atmosphere. This type of aerosol particles is primarily emitted by flaming and smoldering fires together with large amounts of organic aerosols (OA) (Andreae and Merlet, 2001) and is considered an important short-lived climate forcing agent (Andreae, 2001; Bond et al., 2004, 2013). The light absorbing fraction of OA, which is co-emitted with BC, is called *brown carbon* (BrC) (Andreae and Gelencsér, 2006). The BC + BrC aerosol fraction is commonly defined as *light-absorbing carbonaceous* (LAC) matter (Petzold et al., 2013). A list of frequently used acronyms and symbols can be found in Table A1.

During combustion, aerosol particles are co-emitted with carbon monoxide (CO). The ratio between aerosol mass or number concentrations and CO has been used to trace the origin and age of air masses (Guyon et al., 2005; Janhäll et al., 2010). Enhancement ratios (ER_{BC}) for open biomass burning measured for boreal forest smoldering fires have an average ER_{BC} of 1.7 ng m^{-3} ppb^{-1} (Kondo et al.,

2011). In contrast, agricultural fires exhibit higher ER_{BC} compared to forest fires, with reported values varying between 2.2 and 30 ng m^{-3} ppb^{-1} (Mikhailov et al., 2017 and references therein).

Biomass burning plumes are usually dominated by accumulation mode aerosol particles, which are efficient to scatter radiation in the UV-visible range and are also rich in BC. In the absence of BB aerosol particles, the biological coarse mode particles become dominant in terms of mass and the aerosol optical properties are affected (Moran-Zuloaga et al., 2017). Therefore, clear seasonal trends in scattering and absorption have been observed by long-term measurements in the Amazon region (Rizzo et al., 2013).

The light absorption of BC has a wavelength dependence that depends on the BC mixing state, its size distribution and the composition of co-emitted particles (Andreae and Gelencsér, 2006; Kirchstetter et al., 2004; Lack et al., 2013; Schuster et al., 2016). The wavelength dependence is described by the absorption Ångström exponent ($å_{abs}$) (Ångström, 1929). It varies from low values ($å_{abs}$ = 1.0 ± 0.1, weak spectral dependence), usually associated with fossil fuel emitted BC (Bond and Bergstrom, 2006), up to high values ($å_{abs}$ = 6-7, strong spectral dependence) for organic-rich aerosol, e.g., humic-like substances (Hoffer et al., 2006). Measurements at an Amazonian forest site during the dry season resulted in $å_{abs}$ average values below 1.0 for absorption coefficients lower than 15 Mm^{-1} at 450 nm (Rizzo et al., 2011). For BB aerosol particles, the $å_{abs}$ is usually higher than 1.0. However, it depends on the burning conditions, the BC to OA ratio (Saleh et al., 2014), and the BC-BrC size distributions and morphologies (Kirchstetter et al., 2004; Womack et al., 2017). Several studies have used the absorption spectral dependence to apportion the fossil fuel and BB contributions to total absorption (Favez et al., 2010; Massabò et al., 2015; Sandradewi et al., 2008). However, the $å_{abs}$ values do not always reflect the combustion type and using it as a source apportionment parameter can lead to erroneous results (Garg et al., 2016; Lack and Langridge, 2013; Lewis et al., 2008; Wang et al., 2016b). Several studies assume a BC $å_{abs}$ of 1.0 but models show that pure BC could exhibit a broader range of $å_{abs}$ values (Moosmüller et al., 2011). In order to retrieve the ambient BC wavelength dependence, Wang et al. (2016b) proposed the use of the wavelength dependence of $å_{abs}$ instead of $å_{abs}$ itself. The so-called *wavelength dependence of* $å_{abs}$ (WDA) is calculated as the difference of two wavelength pairs; one for short to long wavelengths (e.g., 440 – 870 nm) and another for medium to long wavelengths (e.g., 675 – 880 nm).

Precise BC mass measurements are required to retrieve the correct relationship between absorptivity and BC mass, defined as the mass absorption cross-section (MAC or α_{abs}). The BC mass concentration has traditionally been measured by using thermal or thermal-optical techniques (Cachier et al., 1989; Chow et al., 2007). However, these methods suffer from several biases, like organic carbon charring that increases the apparent BC concentration, especially when high organic fractions are present (Andreae and Gelencsér, 2006). More recently, laser-induced incandescence (LII) techniques have been introduced (Snelling et al., 2005). These techniques measure the volume-equivalent mass of refractory black carbon (rBC) that vaporizes at temperatures of 2800-4000 K. The MAC is used by atmospheric radiative transfer models to obtain absorption coefficients from mass concentration data. The MAC of BC varies between 4 and 11 $m^2 g^{-1}$ at 550 nm, with an average of 6.5 $m^2 g^{-1}$ at 637 nm for fresh soot (Bond and Bergstrom, 2006). In case of condensation of non-BC material on the BC particles, the MAC can be enhanced due to the well-known 'lensing effect' (Fuller et al., 1999). This commonly happens when BC is emitted by BB, since it is co-emitted with large amounts of organic vapors that can condense on BC particles (Saleh et al., 2014). In the central Amazon, black carbon particles have been shown to be coated by organic and inorganic matter (Pöhlker et al., 2014; Pöschl et al., 2010). It has been found that the coating mass significantly affects the absorption enhancement of BC particles, but no significant changes are caused by variations in the coating's oxygen-to-carbon ratio (Tasoglou et al., 2017). A wide range of MAC values can be found in the literature for different fire conditions (smoldering and flaming).

Commonly, the absorption properties of an aerosol population are reported as the single scattering albedo (SSA, ω_0), which is defined as total scattering divided by total extinction (absorption + scattering). Therefore, a lower ω_0 is associated with a stronger absorption. Tropical Amazonian forest fires have moderately high ω_0 values (0.93 ± 0.02 at 670 nm), given the high amount of scattering aerosols which are co-emitted with LAC, compared to African savanna fires that have lower ω_0 values (0.84 ± 0.015 at 670 nm) (Reid et al., 2005). In the Amazon rain forest, long-term measurements by Rizzo et al. (2013) have found similar values for ω_0 during the dry and the wet season, 0.87 ± 0.06 and 0.86 ± 0.09, respectively. The low ω_0 in the wet season is attributed to long-range transported aerosols that include mineral dust and aged BB aerosol particles. Aged BB aerosol is proven to have increased

MAC, and therefore lower ω_0 (Reid et al., 2005). Moreover, the biogenic part of the aerosol can contribute up to 35 % of total light absorption (Guyon et al., 2004).

When present in large amounts in the atmosphere, mineral dust can significantly absorb light, with a MAC of 0.02 – 0.1 $m^2 g^{-1}$ at 550 nm (Clarke and Charlson, 1985). It is mobilized from soils and suspended in the atmosphere by windstorms in areas like the Saharan desert in Africa. Dust aerosol particles in the atmosphere efficiently scatter visible radiation and are able to absorb infrared radiation (Andreae, 1996), having a $\mathring{a}_{abs} >> 1.0$ (Caponi et al., 2017; Denjean et al., 2016). Mineral dust plumes travel over the Atlantic Ocean and are able to reach the American continent. Depending on the circulation patterns over the tropical Atlantic, the African dust plumes will be transported to South America or to the Caribbean Sea and Central America (Prospero et al., 1981). The average transport time from emission to deposition in the Amazon basin during winter is ~10 days (Gläser et al., 2015). Ground measurements of aerosol physical and chemical properties have confirmed that between January and April mineral dust plumes from Africa episodically dominate the aerosol load over large parts of the Amazon rain forest (Formenti et al., 2001; Guyon et al., 2004; Moran-Zuloaga et al., 2017; Talbot et al., 1990; Wang et al., 2016a). Moreover, the dust-enriched aerosol usually arrives together with BB aerosol emitted by fires in sub-Sahelian west Africa and also aerosol particles emitted by industrial activities in Morocco and the western Sahara coast (Moran-Zuloaga et al., 2017; Salvador et al., 2016). In spite of anthropogenic disturbance of soils in Africa that could enhance the flux of mineral dust to the atmosphere (Andreae, 1991), a decreasing trend in mineral dust emissions since the 1980s has been observed and is mainly caused by a reduction of surface winds in the Sahel region (Ridley et al., 2014).

This study provides a comprehensive and in-depth analysis of the aerosol optical properties in the Amazonian atmosphere. A continuous long-term data set (2012 – 2017) of different optical properties is provided. We particularly focus on the impact of BB emissions from long-range transport and from regional/local open fires during the dry season. By using data from another central Amazonian remote sampling site, we extend our time series back to 2008 and provide the longest data set on optical properties measured in the Amazon rain forest so far. By this means, we are able to study the perturbations caused by the El Niño Southern Oscillation (ENSO), which has been reported to cause

droughts in the Amazon Basin (see Fig. S1), with increasing fire activity and forest degradation (Aragão et al., 2007; Cochrane, 2003; Davidson et al., 2012; Lewis et al., 2011).

2 Materials and methods

2.1 Sampling site and measurement period

Aerosol particles and trace gases are being measured at the Amazon Tall Tower Observatory (ATTO) site, located in the Uatumã Sustainable Development Reserve, Amazonas State, Brazil, in central Amazonia since 2011 (Andreae et al., 2015). The large-scale meteorological conditions of the site are determined by the seasonal migration of the inter-tropical convergence zone (ITCZ) (Pöhlker et al., 2018). From August to November, during the *dry season*, the ITCZ is located in the north of South America, and mostly Southern Hemisphere air masses reach the ATTO site bringing BB emissions from deforestation hot-spots in Southeastern Brazil (i.e., so called arc of deforestation) as well as transcontinental emissions from Southern Africa. During the *wet season*, from February to May, when the ITCZ shifts to southern latitudes, the air masses generally come from the northern hemisphere, following a path over the Atlantic Ocean from the African continent and then, over mostly untouched forest areas upwind of the ATTO site. The transition seasons, *dry to wet* and *wet to dry*, occur in December – January and June – July, respectively.

At the ATTO site, systematic aerosol measurements were started in March 2012, being continuously extended and intensified since then. In the course of this process, the aerosol inlet system was modified and upgraded step-wise. A detailed list of the different inlet configurations and characteristics can be found in Table S1. On 04 May 2014, a PM_1 cyclone was installed in the common inlet line for the aerosol optical measurements. The rest of the instrumentation kept sampling total suspended particles (TSP). The sample air was dried by diffusion driers filled with silica gel to guarantee a relative humidity around 40 % or below. An automatic regenerating adsorption aerosol dryer (Tuch et al., 2009) was installed in January 2015.

Another sampling site, ZF2 / TT34 tower, located ~60 km NNW of Manaus and ~140 km WSW of ATTO (Fig. S2), has been the location of long-term aerosol observations and intensive measurement campaigns (Martin et al., 2010a; Rizzo et al., 2013). Given that most of the air masses that reach the ZF2 site are similar to those transported over the ATTO site (Pöhlker et al., 2018), the ZF2 data is usually comparable to the ATTO data and the time series presented in this study can complement previous ZF2 time series already reported for the period 2008 – 2011 (Rizzo et al., 2013). Additionally, two intensive observation periods (IOP) and long-term measurements of the GoAmazon2014/5 experiment took place at several measurement sites in the Amazon Basin, including the ATTO site. More details can be found in Martin et al. (2016, 2017).

2.2 Instrumentation

2.2.1 Aerosol light scattering measurements

Scattering coefficients at ATTO were measured using different nephelometers. Figure S3 shows the measurement periods of the different instruments. The first one was a 3-wavelength integrating nephelometer (Model 3563, TSI, St. Paul, USA) (14 Aug 2012 to 24 Nov 2013). The instrument measures aerosol scattering (σ_{sp}) and backscattering (σ_{bsp}) at 450, 550 and 700 nm (Anderson et al., 1996). Calibrations were periodically done by using CO_2 as span gas. Given the optical configuration of the instrument, the truncation of forward scattered radiation constitutes the largest source of error and was corrected by following the procedure described by Anderson et al. (1996). The estimated error of the nephelometer measurements is 8 % for scattering coefficients in the order of 10 Mm^{-1} (Rizzo et al., 2013). Using an averaging time of 30 min, the detection limit at 550 nm was 0.14 Mm^{-1} (Rizzo et al., 2013).

Later, in February 2014, the TSI nephelometer was replaced by an Aurora 3000 (Ecotech Pty Ltd., Knoxfield, Australia), which measures at 450, 525, and 635 nm wavelength. Over the measurement period studied in this work, we used two different Aurora instruments, with and without backscattering measurement. The Aurora nephelometer was set up to work with an integration time of 1 min. Similar to the TSI nephelometer, CO_2 calibrations were periodically performed. The data was corrected for

truncation according to Müller et al. (2011b). Uncertainty in scattering measurements by the Aurora nephelometers was estimated to be 5 % (Müller et al., 2011b).

2.2.2 Aerosol light attenuation and absorption measurements

Light absorption coefficients at 637 nm wavelength, $\sigma_{ap\,637}$, were measured by a multi-angle absorption photometer, (MAAP, model 5012, Thermo Electron Group, Waltham, USA). This instrument measures the transmission of light through a glass-fiber filter on which aerosol particles are collected. Additionally to the forward hemisphere transmission measurement, the MAAP measures the light back scattering at 130° and 165°. By using a radiative transfer model (Petzold and Schönlinner, 2004), the instrument is able to provide absorption coefficients. The instrument was set up to provide data at 1-min resolution. By averaging the data at 30-min intervals, the MAAP detection limit is 0.13 Mm^{-1}, which corresponds to a BC_e mass concentration of 20 ng m^{-3} (calculated with a MAC of 6.6 $m^2\ g^{-1}$). The MAAP was generally operated at a flow rate of 10 L min^{-1}, but for some periods the flow rate was reduced to 8.3 L min^{-1}. According to Müller et al. (2011a), the MAAP measures at a wavelength of 637 ± 1 nm, instead of the 670 nm reported in the instrument's manual. In our calculations, we use 637 nm as the default MAAP wavelength and do not apply any interpolation factor to scale up the data from 670 to 637 nm since it would be within the instrument's ~5 % uncertainty range. The total uncertainty of the MAAP absorption measurements is of the order of 10 % for 30-min average times (Rizzo et al., 2013).

An aethalometer was used to measure attenuation of light by aerosol particles at different wavelengths. This instrument uses an LED light source to irradiate an aerosol-laden quartz-fiber filter and a detector, located in the forward hemisphere, to measure the light transmission (Hansen et al., 1984). The measured transmission is compared to a blank measurement in order to obtain a change in light transmission (i.e., attenuation). This attenuation is then converted to BC mass concentration by using a mass attenuation cross section that depends on the instrument model (14625 and 6837.6 $m^2\ g^{-1}\ \lambda^{-1}$ for the AE31 and AE33 Aethalometer models, respectively).

Aethalometer measurements started at the ATTO site in April 2012 using a model AE31 (Magee Scientific, Berkeley, USA). The instrument was operated at different flow rates during the measurement

period (varying from 2.0 to 3.7 L min^{-1}) and measured attenuation every 15 min. In January 2015, a new Aethalometer, model AE33 (Aerosol d.o.o., Ljubljana, Slovenia), was installed. The overlapping measurement time of the AE31 and the AE33 models (27 Nov to 15 Dec 2014) enabled the comparison of both data sets. We found good agreement between both models (difference < 10 %) for measurements at 470, 520, 590, and 660 nm. However, the wavelength dependence did not fit very well during this intercomparison period. Similar deviations in the wavelength dependence of AE31 and AE33 have been reported previously (ACTRIS, 2014). Nevertheless, it is still not clear if the higher wavelength dependence of the AE33 compared to the AE31 is the result of an artifact of the instrument. An independent multi-wavelength absorption measurement can help to clarify the aforementioned AE31/AE33 deviation in $\mathring{a}_{abs}$ (Saturno et al., 2017b). The comparison between compensated AE31 and AE33 data was used to correct the AE33 wavelength dependence deviation by applying intercomparison factors to AE33 data. The obtained AE31-AE33 intercomparison fits are shown in Fig. S4.

Aethalometer data require several corrections to account for different artifacts related to multiple scattering by the filter fibers, scattering by embedded aerosol particles and filter loading effects. The correction applied in this study has been described in a previous article (Saturno et al., 2016). The compensation algorithm is based on the correction scheme proposed by Collaud Coen et al. (2010). It uses MAAP data as a reference absorption measurement, which could introduce uncertainties related to the modification that aerosol particles can suffer by being deposited on a filter matrix. We retrieved the $\mathring{a}_{abs}$ from applying a log-log fit to Aethalometer data corrected for filter-loading and multiple scattering effects. In the case of the Aethalometer AE33, the measurements do not require a filter-loading correction because this model uses the dual-spot technology which accounts for this artifact (Drinovec et al., 2015). The AE33 internal algorithm applies a multiple scattering correction using the correction factor reported by Weingartner et al. (2003). In this study, this compensation was reverted and the multiple scattering correction was calculated according to a comparison with MAAP measurements, in a similar fashion to the one applied to AE31 data, mentioned above.

2.2.3 rBC mass measurements and MAC calculations

Refractory black carbon (rBC) was measured using a single particle soot photometer (SP2) revision C (Droplet Measurement Technologies, Longmont, USA). Initially, the measurements were done with a 4-channel SP2 and the instrument was upgraded on 19 January 2015 to the 8-channel configuration. Figure S3 shows the different measurement periods of this instrument. The SP2 uses a high-intensity Nd:YAG laser beam (1 MW cm^{-2}, λ = 1064 nm) to irradiate aerosol particles that are provided by an air jet at 90°, with a flow rate of 0.12 L min^{-1}. All particles scatter the light from the laser beam and some of them, which are able to absorb radiation at the given wavelength (e.g., rBC), will incandesce and vaporize at high temperatures (Moteki and Kondo, 2008; Stephens et al., 2003). Four avalanche photo-diode (APD) detectors are installed in the instrument to measure a) scattering, b) broadband incandescence (350 – 800 nm), c) narrowband incandescence (630 – 880 nm) and d) scattering with a split detector. Time dependent data is recorded from each particle as it passes through the laser beam. The ratio between broadband and narrowband signals can provide information on the particle's composition since it is related to the boiling point temperature of the sampled particles (Schwarz et al., 2006). The instrument was periodically calibrated using fullerene soot (Alfa Aesar Inc.) as rBC reference material. A quadratic fit was applied to the recorded incandescence peak heights vs. the mass of mobility size-selected fullerene particles. The fullerene effective densities were taken from Gysel et al. (2011). The scattering detector was calibrated using polystyrene latex spheres (PSL) by relating the scattering signal to the PSL scattering cross-section. The SP2 rBC dynamic ranges were 80 – 280 nm and 80 – 450 nm for the 4-channel and the 8-channel configurations, respectively.

The narrow dynamic range of the 4-channel SP2 was preventing us from measuring rBC mass concentration values comparable to MAAP measurements. In a comparison with another 8-channel instrument during the GoAmazon2014/5 experiment we found that the 4-channel instrument was underestimating the rBC mass concentration by a factor of 40 %. This factor was stable during the wet season 2014 but we could not measure its stability during the following dry season. Due to instability of this factor over the sampling period, a proper data correction was not possible. Therefore, in this paper we use only the 8-channel instrument's data, which were available from 09 February 2015 until 31 July 2016 with some interruptions due to hardware failures. The 8-channel SP2 rBC size-dependent counting

efficiency was obtained by comparing the counts of fullerene particles measured by the SP2 and a condensation particle counter (CPC). This way, an underestimation factor of 5 % was found to affect SP2 rBC mass measurements and a scaling factor of 1.05 was applied to the data to account for this systematic error. Similar underestimation factors have been previously reported (Liu et al., 2017; Wang et al., 2014). The cumulative uncertainty of the SP2 measurements associated with the counting efficiency and mass calibration of the instrument has been estimated to be around 25 % (Wang et al., 2014).

The BC mass absorption cross-section, α_{abs}, was calculated by running daily fits of 30-min averaged MAAP $\sigma_{ap\,637}$ vs. SP2 rBC mass concentration data, using a standardized major axis estimation (as explained in section 2.6). Fits with $R^2 < 0.9$ were filtered out resulting in a total of 106 out of 220 days included in the final result. Given the mentioned SP2 and MAAP uncertainties, the α_{abs} values presented here have uncertainties around ±40 %. The obtained α_{abs} values (shown in section 3.1) were used to convert MAAP absorption measurements into BC_e mass concentrations.

2.2.4 Complementary measurements

Online chemical composition of aerosol particles has been measured since August 2014 using an aerosol chemical speciation monitor (ACSM) (Aerodyne Research Inc., Billerica, USA). Initial results on non-refractory aerosol chemical composition at the ATTO site have already been reported by Andreae et al. (2015) and a detailed paper on the long-term ACSM observations is being prepared by Carbone et al. (2017). This online mass spectrometry technique detects organics, nitrate, sulfate, ammonium and chloride in the sub-micron (< 1 μm) aerosol size range (Ng et al., 2011).

A Picarro cavity ring-down spectrometer G1302 analyzer (Picarro Inc., Santa Clara, USA) measured CO_2 and CO at the ATTO site. Three calibration tanks were used to calibrate the instrument every 100 h. A Nafion™ dryer was installed in front of the instrument in order to reduce the noise in the CO measurements, which are affected by the high relative humidity of the tropical forest air. Calibration and performance checks will be reported in an upcoming paper. The instrument samples at five different heights but we restrict our analysis to the data measured at 79 m. All CO measurements have been

conducted on the walk-up tower. The measurement setup is largely inspired by a setup operational at another location since 2009 (see Winderlich et al., 2010). In order to calculate the BC enhancement ratios with respect to CO (ER_{BC}), we used a major axis estimation fit that was applied to the bivariate data (Falster et al., 2006) where the slope represents the enhancement ratio. The 5th percentiles were used as background values.

Condensation nuclei (CN) number concentrations, N_{CN}, and size distributions from 10 nm to 10 µm were continuously measured using several instruments including mobility and optical particle sizers [more details can be found in Andreae et al. (2015)]. In this study, we used coarse mode (> 1 µm) number and mass concentrations obtained by means of an optical particle sizer (OPS) model 3330 (TSI Inc., Shoreview, USA) to identify mineral dust transport events. A detailed analysis of the Saharan dust plume arrivals at the ATTO site can be found in Moran-Zuloaga et al. (2017). Aerosol particle size distributions (10 – 430 nm diameter) were measured with a scanning mobility particle sizer (SMPS) models 3080 and 3081 (TSI Inc., Shoreview, USA) using a CPC, model 3772 (TSI Inc., Shoreview, USA).

2.3 Wavelength dependence and BrC contribution calculations

Light scattering and absorption wavelength dependence are represented by the Ångström exponents, $å_{sca}$ and $å_{abs}$, respectively. The Ångström exponent can be retrieved when measurements at two or more different wavelengths are available, for example, the $å_{abs}$ can be calculated as

$$å_{abs} = -\frac{\ln\left(\frac{\sigma_{ap}(\lambda_1)}{\sigma_{ap}(\lambda_2)}\right)}{\ln\left(\frac{\lambda_1}{\lambda_2}\right)}, \qquad (1)$$

where σ_{ap} is the absorption coefficient at two different wavelengths, λ_1 and λ_2.

When measurements at more than two wavelengths are available, a linear fit can be used to retrieve the Ångström exponent from the logarithm of the absorption (or scattering) coefficients vs. the logarithm of the wavelength, as follows

$$\ln \sigma_{ap} = -\mathring{a}_{abs} \ln(\lambda) + \ln(\text{constant}) \quad , \qquad (2)$$

Black carbon is commonly taken to be wavelength-independent with $\mathring{a}_{abs} = 1$. However, this assumption is theoretically wrong and the BC-related $\mathring{a}_{abs}$ is very sensitive to the size of the particles (Moosmüller et al., 2011). Wang et al. (2016b) proposed a method to calculate the *wavelength dependence of the Ångström exponent* (WDA) in order to estimate the BrC contribution to total light absorption by aerosol particles. They use the difference between two $\mathring{a}_{abs}$ calculated for two different wavelength pairs (440 – 870 nm, and 675 – 880 nm) using aerosol robotic network (AERONET) and Aethalometer data. We use a similar approach to retrieve WDA using Aethalometer data from the ATTO site. In this study the WDA is calculated as follows:

$$\text{WDA} = \mathring{a}_{\text{abs 370-950}} - \mathring{a}_{\text{abs 660-950}} \quad , \qquad (3)$$

where $\mathring{a}_{\text{abs 370-950}}$ and $\mathring{a}_{\text{abs 660-950}}$ correspond to the absorption Ångström exponents calculated for the 370 – 950 and 660 – 950 nm wavelength pairs, respectively. This way, a theoretical BC WDA was calculated from the modeled $\mathring{a}_{abs}$ for BC (BC WDA= $\mathring{a}^{BC}_{\text{abs 370-950}}$ - $\mathring{a}^{BC}_{\text{abs 660-950}}$).

Theoretical WDA values were calculated following conceptual Mie theory models for (i) polydisperse BC particles (Mishchenko et al., 1999), and (ii) core-shell internally mixed monodisperse BC (Bohren and Huffman, 1983). Characteristic BC core size distributions measured by the SP2 during the wet and dry season were used in the polydisperse BC-only model to retrieve extinction efficiency and single scattering albedo. The refractive indices used were 1.95 - 0.79i for BC (Bond and Bergstrom, 2006) and 1.55 - 0.001i for the coating material (Liu et al., 2015). The latter value was only used for the internally mixed BC case. The BC core diameters used in the internally mixed case were 100, 125, 150, 175, 200, 225, and 250 nm, with coating thickness to core size ratio from 0.1 to 1. These values are in accordance with rBC mass size distributions observed at the ATTO site, see Fig. S5. Black carbon density was set to 1.8 g cm^{-3} (Schkolnik et al., 2007). Calculated BC WDA thresholds (25th and 75th percentiles), shown in Fig. S6, were compared to the ambient data in order to identify BrC influenced periods. For a general analysis, data with WDA lower than the 75th percentile were considered to be in the *BC-only* regime. The presence of BrC, additional to BC, occurred when the modeled BC absorption at 370 nm was exceeded. A sensitivity study of this model was done by changing the refractive indices and the core

size of the model input. These results are presented in Table S2 as relative overestimation of the BrC contribution to $\sigma_{ap\ 370}$. The calculated BC absorption Ångström exponents ($\mathring{a}^{BC}_{abs}$) for the two wavelength pairs mentioned in Eq. (3) were used to calculate BrC absorption at 370 nm, as follows:

$$\sigma^{BC}_{ap\ 370} = \sigma_{ap\ 950} \times \left(\frac{370}{950}\right)^{-\mathring{a}^{BC}_{abs\ 370\text{-}950}}, \quad (4)$$

$$\sigma^{BrC}_{ap\ 370} = \sigma_{ap\ 370} - \sigma^{BC}_{ap\ 370}, \quad (5)$$

where $\mathring{a}^{BC}_{abs\ 370\text{-}950}$ is obtained from the Mie model calculations. The uncertainties of the BrC contribution to total absorption at 370 nm were calculated using the theoretical minimum and maximum BC WDA values. They were below 37 % overall, and decreased to below 19 % when the BrC contribution was higher than 30 % at 370 nm. The relative overestimation of the BrC contribution obtained by using different BC core sizes and different refractive indices in the Mie model calculations can be found in Table S2.

2.4 HYSPLIT backward trajectories and clustering

The systematic backward trajectory (BT) analysis used here is described in Pöhlker et al. (2018). Briefly summarized: Three-days backward trajectories were calculated by running the NOAA hybrid single-particle Lagrangian integrated trajectory (HYSPLIT) model (Draxler and Hess, 1998) using 1-degree resolution meteorological data from the global data assimilation system (GDAS1). The trajectories were calculated for 1000 m above ground level at 1 hour intervals for the period January 2008 to June 2016. The entire trajectory ensemble was classified into 15 BT clusters using a k-means cluster analysis. The clusters represent different air mass transport tracks and velocities. The different cluster average trajectories and their frequency of occurrence are shown in Fig. 1a and 1b, respectively. The clusters are classified as northeasterly ("NE1", "NE2", and "NE3"), east-northeasterly ("ENE1", "ENE2", "ENE3", and "ENE4"), easterly ("E1", "E2", "E3", and "E4), southeasterly ("ESE1", "ESE2", and "ESE3"), and southwesterly ("SW1") trajectory clusters. In some parts of the analysis presented here the trajectory clusters are grouped by main directions (NE, ENE, E, and ESE).

South American fire count data were retrieved from the satellite observations database available online by the Instituto Nacional de Pesquisas Espaciais (INPE), Brazil, at https://prodwww-queimadas.dgi.inpe.br/bdqueimadas/, last access on 04 Apr 2017. The fire data covered the same period as the HYSPLIT clustering analysis period, January 2008 to June 2016. Fire counts were classified at hourly resolution according to the corresponding BT cluster where they occurred. The fire counts reported in this study were weighted according to the trajectory density as (trajectory counts) / 100 km^2. Since the fire count number depends on the amount of satellite data available, we use these data with caution and only as a qualitative reference. For an extended discussion on fire geographical locations and land cover types, see Pöhlker et al. (2018).

2.5 Satellite data

The aerosol optical depth (AOD) at 550 nm, measured by the moderate resolution imaging spectroradiometer (MODIS) on board of the satellites Terra and Aqua, was retrieved for two domains of interest (see Fig. 2a):

- DOI1: Over the Atlantic Ocean. Used to monitor the westward transport of BB aerosol particles from southern Africa, which are mostly emitted during the Amazon dry season, especially between August and September (Das et al., 2017). There is no guarantee that the observed aerosol over this area will necessarily reach the ATTO site, but it is used as an indication of LRT events from southern Africa that will likely reach the Amazon Basin.
  Boundaries: 30°W; 20°S; 10°W; 0°S.
- DOI2: Over the southern Amazon. Used to monitor BB in this region where fire activity is related to deforestation and agriculture-related activities.
  Boundaries: 58°W; 14°S; 40°W; 8°S.

The MODIS products can be found online on the Goddard Earth Science Data and Information Services Center at https://giovanni.gsfc.nasa.gov/giovanni/, last access on 17 Jul 2017, (GES-DISC, 2017).

Terra and Aqua data were averaged over the two different domains. The averaged AOD at 550 nm time series corresponding to DOI1 and DOI2 can be found in Fig. 2b. The seasonality observed for both

datasets is similar but the AOD for DOI1 (Atlantic Ocean) generally increased in August and decreased after the end of September with some peaks in January – February, especially in 2016. On the other hand, high AOD values in DOI2 (southern Amazon), increased sharply in the beginning of September and decreased continuously until the middle of December with the exception of the dry season 2015 when high AOD was observed until February 2016.

2.6 Data treatment

The analyzed data were averaged to 30-min intervals and corrected to standard temperature and pressure (STP, 273.15 K and 1013.25 hPa). Furthermore, the scattering data were interpolated to 637 nm to compare directly to the absorption data obtained by the MAAP, in order to avoid the uncertainty associated with the absorption spectral dependence calculation. The time periods of major and medium dust influence were taken from a study by Moran-Zuloaga et al. (2017). During the dry season, BB pulses were segregated by using the 75th percentile of $\sigma_{ap\,637}$ as a threshold. When examining correlations between independent measurements, we applied standardized major-axis estimations (SMA) by using the SMATR package (Falster et al., 2006) in the statistical software environment R (R Development Core Team, 2009). This method minimizes the error on the *x* and *y* axes and not only at the *y* axis, like a linear regression does. Therefore, it provides unbiased estimates of the slope (Warton et al., 2006).

3 Results and discussion

3.1 Overview of aerosol optical properties (2012 – 2017)

This section summarizes the aerosol optical properties from five years of continuous measurements at the ATTO site. The corresponding time series are shown in Fig. 3 and descriptive statistics can be found in Table 1. The wet and dry season statistics were calculated excluding the transition periods.

The scattering coefficients, σ_{sp}, are shown in Fig. 3a, averaging 7.5 ± 9.3 Mm^{-1} and 33 ± 25 Mm^{-1} at 550 nm during the wet and the dry seasons, respectively (see Table 1). These values agree well with

previously reported results at ZF2 of 8.1 ± 7.2 Mm^{-1} and 36 ± 48 Mm^{-1} at 550 nm during the wet and dry season, respectively (Rizzo et al., 2013). Good agreement was also found for our results at 450 nm and 700 nm and the corresponding data from Rizzo et al. (2003). The proximity of both sites, ATTO and ZF2, frequently allows probing comparable air masses of similar origin and atmospheric history. The long-term measurements show also a pronounced year-to-year variability in σ_{sp} (compare e.g., 2014 and 2015 in Fig. 3a). The largest observed deviations from the dry-season average were found during the dry season 2015 with an average increase of 38 % in σ_{sp} at 550 nm. Similar increases were observed in σ_{sp} at 450 and 637 nm. These increases can be directly related to the higher occurrence of fire episodes during the strong ENSO period 2015/6 with its negative precipitation anomaly, as discussed in more detail in sections 3.5 and 3.6.

The absorption coefficients, σ_{ap}, at 637 nm (MAAP) are shown in Fig. 3b, and averaged 0.68 ± 0.91 Mm^{-1} and 4.0 ± 2.2 Mm^{-1} during the wet and the dry season, respectively. Also for this parameter, comparable values were measured at the ZF2 site, with averages of 1.0 ± 1.4 Mm^{-1} and 3.9 ± 3.6 Mm^{-1} at 637 nm during the wet and the dry seasons, respectively (Rizzo et al., 2013). The higher increase of the absorption coefficient (factor of 5.9) from wet to dry season compared to the increase in scattering (factor of 4.4) affected the ω_0 (see Fig. 3c). Lower values were observed during the dry season (0.87 ± 0.03 at 637 nm, 0.81 ± 0.08 at 550 nm) compared to the averages observed in the wet season (0.93 ± 0.04 at 637 nm, 0.88 ± 0.08 at 550 nm). At the ZF2 site, Rizzo et al. (2013) have found small differences between ω_0 values during the dry and wet seasons (0.87 ± 0.06, and 0.86 ± 0.09 at 637 nm, respectively) for over 2 years (2008 – 2011) measurements. However, measurements during the wet season in 1998 at a sampling site closer to ATTO (Balbina, 60 km NW of ATTO and 140 km NE of Manaus) showed higher ω_0 values: 0.92 – 0.95 at 550 nm (Formenti et al., 2001). These values are within our measurement range for the same season (0.88 ± 0.08 at 550 nm). Single scattering albedo retrieved from multi-year ground-based radiometer measurements in the Amazonian forest had an average of 0.93 ± 0.02 (Dubovik et al., 2002). Given that we sampled dried aerosol particles, our average ω_0 are expected to be lower than these ambient-humidity values during the entire measurement period and the dry season. Measurements close to BB sources in Brazil have shown a wide range of ω_0; e.g., Chand et al. (2006) found a ω_0 of 0.92 ± 0.02 (550 nm) for dried aerosol over Rondônia, whereas

Guyon et al. (2003) calculated lower ω_0 values during BB events at the end of the LBA-EUSTACH 1 campaign in Rondônia, reaching 0.85 ± 0.02 at 550 nm. Freshly emitted smoke has even lower ω_0, of 0.79 ± 0.05 at 550 nm (Reid et al., 1998).

The scattering Ångström exponent, $å_{sca}$, is a function of the aerosol particle size distribution. However, some studies have found that this relationship is only evident for surface and volume mean diameters and was not clearly valid between $å_{sca}$ and count mean diameters (Rizzo et al., 2013; Virkkula et al., 2011). We obtained higher $å_{sca}$ values during the dry season (1.71 ± 0.24) compared to the wet season (1.29 ± 0.50) as shown in Fig. 3d. This is an indication of the dominance of fine mode aerosol (mostly BB related) during the dry season over the coarse mode aerosols that become more important in the wet season (i.e., PBAP, Saharan dust and sea salt), as previously observed at the ATTO site (Andreae et al., 2015; Moran-Zuloaga et al., 2017). A similar seasonal trend has been observed at the ZF2 site, where $å_{sca}$ was 1.70 ± 1.41 and 1.48 ± 1.12 (30-min averages) for the dry and the wet season, respectively (Rizzo et al., 2013). A detailed analysis of the coarse mode aerosol abundance and properties measured at the ATTO site is presented elsewhere (Moran-Zuloaga et al., 2017).

Regarding the absorption Ångström exponent, $å_{abs}$, the overall average during the whole sampling period was 0.93 ± 0.16 (see Fig. 3e). Although no significant difference was found between dry and wet season averaged values, the averaged $å_{abs}$ was slightly higher during the dry season, reaching 0.94 ± 0.16 compared to 0.91 ± 0.19 during the wet season. It was found that the $å_{abs}$ only increased significantly during hours or days-long episodes, typically caused by nearby burning during the dry season. Details on the absorption wavelength dependence are discussed in section 3.7. The Aethalometer compensation calculation could potentially affect the retrieved $å_{abs}$ values. It has been shown that the raw attenuation Ångström exponent can represent a good approximation to the real $å_{abs}$ (Saturno et al., 2017b). High absorption and scattering coefficients coincide with ESE and E trajectories, which are mostly dominant, but not exclusively, during the dry season, see Fig. 1. On the other hand, the "cleanest" periods in the wet season, when light absorption reaches its minimum and ω_0 its maximum, the dominant trajectories are ENE and NE.

3.2 Black carbon mass absorption cross-section

Accurate MAC values are required to retrieve BC mass concentrations from absorption measurements. During the entire measurement period, the calculated MAC was 11.9 ± 1.4 $m^2\ g^{-1}$ (mean ± standard deviation) at λ = 637 nm. Daily calculated MAC values in the wet season were slightly lower on average compared to the dry season values (11.4 ± 1.2 and 12.3 ± 1.3 $m^2\ g^{-1}$, respectively, see Table 1). As an illustration of the different MAC values obtained in the wet and the dry seasons, $\sigma_{ap\ 637}$ vs. M_{rBC} scatter plots are presented as supplementary information in Fig. S7. Lower MAC values measured in the wet season 2016 could be associated with less coated BC compared to more aged particles in the dry season, which could have thicker coatings. Nevertheless, both values are much higher than the 6.6 $m^2\ g^{-1}$ suggested by Bond and Bergstrom (2006), especially considering that mineral dust and BrC do not strongly absorb at this wavelength and would therefore have little influence on the apparent MAC. However, they are in agreement with a modelled absorption enhancement of 1.6 calculated for open biomass burning in Brazil (Liu et al., 2017). In any case, there are large discrepancies that make it difficult to compare different MAC values obtained from ambient measurements due to systematic analytical uncertainties that dominate over the natural variability (Zanatta et al., 2016). These uncertainties are introduced by filter-based absorption measurement biases and BC mass over- or underestimation when thermal optical methods are used. In the case of the SP2, the rBC mass measurements are free of the different biases that affect thermal-optical techniques and are a wavelength-independent measurement. In the case of absorption measurements, a positive bias is introduced when organic aerosol deposits on the filter, enhancing the scattering by the filter fibers and the absorption by previously deposited BC particles when coating them. This artifact can be between 12 and 70 % for particle soot absorption photometer (PSAP) measurements and will depend on the OA to BC ratio and the aging state of the organic aerosol particles (Lack et al., 2008). We expect a lower artifact for the MAAP since the scattering by filter fibers is accounted by the reflectance measurements, but using our instrumentation we are not able to estimate the artifact coming from embedded BC absorption being modified by organic aerosol deposition. There are only few field studies that present comparisons of rBC measurements and light absorption measurements, like MAAP, photoacoustic spectrometry (PAS), or Aethalometer, and especially long-term measurements are scarce. Raatikainen

et al. (2015) reported SP2 (8-channel) and MAAP measurements in the Finnish Arctic and found that SP2 rBC mass concentrations were 5 times lower than MAAP BC_e mass concentration measurements, which is equivalent to MAC values of ~30 $m^2\ g^{-1}$ at 637 nm. Some other studies have found values in closer agreement with our ATTO MAC results. For example, Laborde et al. (2013) found that air masses over Paris had an average MAC of 11.9 and 10.8 $m^2\ g^{-1}$ (interpolated to 637 nm), for aged and fresh BB aerosol, respectively. Additionally, Liu et al. (2010) calculated a median MAC of $10.2 \pm 3.2\ m^2\ g^{-1}$ during a measurement campaign at the Jungfraujoch research station in Switzerland. Another study in Mexico City, using PSAP for absorption measurements at $\lambda = 660$ nm, found a MAC of 11.2 $m^2\ g^{-1}$ (interpolated to 637 nm) (Subramanian et al., 2010).

3.3 Variability of optical properties during the dry season

The Amazonian dry season is generally impacted by BB aerosol particles that cause an increase in scattering and absorption coefficients (see Fig. 3a-b). However, the aerosol optical properties vary with the burning material (and region), as well as the aging process prior to reaching the ATTO site. In order to study the dry season variability of BB aerosol particles, multi-year (2012 – 2017) weekly averages were analyzed. The air mass trajectories, presented as BT clusters in Fig. 4a, show a decreasing dominance of ESE winds from August to November, whereas from October to November there is an increasing influence of ENE winds, indicating the south-to-north air mass trajectory shift that occurs during the transition from the dry to the wet season. It is important to note that southerly and easterly winds are most likely to bring BB aerosol to the ATTO site during the dry season, given that very active open fire areas during this period are located in the southern Amazon and the Cerrado region (Andreae et al., 2012; Guyon et al., 2005) and, more remotely, in southern Africa (Andreae et al., 1994; Barbosa et al., 1999; Das et al., 2017). Aerosol optical depth at 550 nm is used in this study as a parameter to study the seasonal pattern of BB emission transport from both areas. In section 2.5, we defined two domains of interest to study the aerosol seasonal patterns in these two areas: DOI1 for the LRT of South African smoke over the Atlantic Ocean, and DOI2 for the fires occurring in the southern Amazon. For the southern Africa fires (DOI1), the seasonal pattern shows an important influence during August – October, slightly decreasing towards the end of the Amazonian dry season (see Fig. 4d). For

the southern Amazon region (DOI2), the typical fire seasonality during the dry season is observed in the AOD over this area (Fig. 4d) with the highest values observed in September and October. It is important to note that August seems to be the period when African LRT is a more important source than regional emissions and could be considered as the main contributor of BB aerosol to the ATTO site during this time. For the rest of the dry season, it is likely that the aerosol properties are defined by South American BB emissions. In fact, the shift in air mass trajectories and variation of BB sources drive the BrC contribution to $\sigma_{ap\,370}$, as shown in Fig. 4b. The BrC contribution (associated with high $\mathring{a}_{abs}$) is more important at the end of the dry season and is lower during August, when the aerosol particles likely arrive from Zambian woodland savanna fires (Barbosa et al., 1999), which burn more efficiently and emit aerosol particles with lower ω_0, 0.84 ± 0.015 at 670 nm on average (Dubovik et al., 2002). Additionally, on average, high $\sigma_{ap\,637}$ events (see increasing circle size in Fig. 4b) are more likely to bring high BrC containing aerosol, which is another indication that closer fires have higher probability to provide BrC-rich aerosol particles to the ATTO site. The absorption wavelength dependence and BrC contribution are discussed in detail in section 3.6. The differences between both identified BB sources in terms of BrC can be explained by two reasons: (i) the BrC photochemical oxidation and destruction of chromophores during transport (Sumlin et al., 2017) that would strongly affect LRT aerosol, and (ii) a lower rain scavenging rate for BC during transport, which would lead to an increased BC fraction in the aerosol population. The increase of the single scattering albedo (ω_0, Fig. 4c) towards the end of the dry season confirms that the aerosol particles during this time are scattering more radiation, not only due to higher BrC presence but also due to other light-scattering aerosol particles.

3.4 Diel cycles

Figure 5 presents the diel cycles observed during the dry and the wet seasons for the following selected aerosol properties and meteorological parameters: Accumulation mode particle number concentration ($N_{acc,}$), absorption coefficient at 637 nm ($\sigma_{ap\,637}$), BrC absorption coefficient at 370 nm ($\sigma_{ap\,BrC\,370}$), precipitation rate (P_{ATTO}), and equivalent potential temperature (θ_e). In order to study the typical diel cycles in each season, extreme events like mineral dust transport in the wet season and nearby BB during El Niño in 2015 – 2016 have been excluded by using data within the 90% confidence interval.

The diel cycle of the equivalent potential temperature (Fig. 6i-j), calculated according to Stull (1988), reflects the evolution of the planetary boundary layer (PBL). Shortly before sunrise (~ 10:00 UTC), θ_e exhibits its minimum and increases afterwards reaching its maximum values in the early afternoon hours. The pronounced increase in θ_e in the early morning hours reflects the onset of solar warming and the initiation of vertical mixing, leading to the evolution of the convective boundary layer. After sunset, a stable nocturnal boundary layer is formed close to the forest canopy. A detailed analysis of the planetary boundary layer of the Amazon can be found in Fisch et al. (2004). Figures 5a-b show diel cycles of accumulation mode (100 – 430 nm) particle number concentration, N_{acc}. The diel patterns are similar during both seasons, with a minimum at sunrise, and an increase that starts in the morning at 12:00 UTC (8:00 LT) and maximum concentrations between 17:00 and 18:00 UTC (13:00 – 14:00 LT). This diel pattern observed in N_{acc} is driven by the diurnal evolution of the planetary boundary layer. On the one hand, the stable nocturnal layer leads to a concentration of particles and gases close to the canopy. On the other hand, the canopy acts as an effective particle sink, resulting in a concentration decrease towards the early morning (Ahlm et al., 2009). After sunrise, vertical mixing breaks up the stable nocturnal boundary layer. While the subsequent increase in N_{acc} is likely due to entrainment of particles from the elevated aerosol-rich layers, the decrease in the afternoon hours can be attributed to effective deposition in the forest canopy, as also discussed in Ahlm et al. (2009). The absorption coefficient at 637 nm, $\sigma_{ap\,637}$, which is mostly related to BC, follows a diel pattern (Fig. 5c-d) similar to the N_{acc} trend for both seasons. Since BC is usually not emitted by nearby sources and it is generally transported in the accumulation mode, the similarities with N_{acc} diel patterns were expected. However, the wet season diel cycle of $\sigma_{ap\,637}$ exhibits a decreasing tendency that starts two hours earlier than the decrease in N_{acc}. This difference can be explained by the fact that $\sigma_{ap\,637}$ and N_{acc} are mass and number-related measurements, respectively. Therefore, a size-dependent deposition would affect mass and number-related aerosol properties differently. This difference was more evident in the wet season when BC concentrations were not as dominant as in the dry season. The diel pattern of BrC contribution during the dry season is significantly different from the $\sigma_{ap\,637}$ (BC) pattern. Brown carbon absorption at 370 nm, $\sigma_{ap\,BrC\,370}$, shows its highest values between 12:00 and 14:00 UTC (08:00 – 10:00 LT) in the dry season and starts decreasing at 14:00 UTC (10:00 LT), earlier than $\sigma_{ap\,637}$ and N_{acc} (Fig. 5e). This

observation implies that the BrC aerosol particles measured at the ATTO site are mixed down into the boundary layer in the early morning and are then quickly photo-degraded during the day (Forrister et al., 2015; Laskin et al., 2015; Rincón et al., 2010; Wang et al., 2016b; Wong et al., 2017).This pattern is not observed during the wet season, when $\sigma_{ap\ BrC\ 370}$ exhibits no significant diel variability.

Other remote site observations have found no significant diel variation of the absorption coefficient, due to efficient mixing of the PBL and low anthropogenic emissions (Chi et al., 2013). At ATTO, the high convectivity and related entrainment of high altitude air masses, containing regional and/or LRT aerosols, result in a pronounced diel cycle in σ_{ap}. This is in good agreement with previous dry season results from another Amazonian site (Brito et al., 2014).

3.5 BC to CO enhancement ratio

Agricultural clearing fires, like savanna fires, are dominated by the flaming combustion phase, in contrast to deforestation fires, where less than 50 % of the biomass is burned in the flaming phase (Dubovik et al., 2002). An important part of forest fires occurs in the form of smoldering combustion due to higher fuel moisture and larger fuel diameters (Guyon et al., 2005). Under smoldering fire conditions, when the combustion is less efficient and thus, tends to emit more CO, observations tend to show lower ER_{BC} and higher single scattering albedo, ω_0, as well as higher organic carbon (OC) enhancement ratio, ER_{OC}. On the other hand, flaming fires, which produce abundant BC aerosol particles, tend to exhibit lower ω_0 and higher ER_{BC} (Akagi et al., 2011). The smoke that arrives at the ATTO site during the dry season is a mixture of smoldering and flaming emissions with varying relative fractions. The air mass origin, (i.e., the backward trajectories) largely defines if emissions are advected from regions with predominantly smoldering or flaming fires (Pöhlker et al., 2018).

The ER_{BC} and ω_0 values allow us to distinguish between flaming and smoldering-derived smoke and help locate the different sources. Figure 6 shows the ER_{BC} and ω_0 values at ATTO, being classified by grouped BT clusters. Mainly, the ESE and E trajectory clusters have ER_{BC} higher than 8 ng m^{-3} ppb^{-1}. From the two predominant BT cluster groups in the dry season (ESE and E), the ESE trajectories seem to be more influenced by flaming fires since the measurements are more shifted to high ER_{BC} and lower

ω_0. In fact, the ESE clusters are dominated by the 0.80 – 0.90 ω_0-range, which means they are highly loaded with light-absorbing aerosol. This is consistent with the land cover information, which indicates that agricultural lands account for 6 – 20 % of the ESE clusters total land cover, 3 – 5 % of the E clusters, and < 1 % of the ENE and NE clusters (Pöhlker et al., 2018). The eastern clusters (E) are more equally distributed in the ω_0 range and tend to be lower in terms of ER_{BC} compared to the ESE clusters. Therefore, we expect E trajectories to be more influenced by smoldering fires during the dry season compared to the ESE trajectories, even though, as already mentioned, the arrival of African savanna fire smoke from easterly trajectories in August-September provides BB aerosol particles that have lower ω_0 and higher ER_{BC}.

During the wet season, when ENE and NE BT clusters are dominant, we observed a trend towards lower ER_{BC} and higher ω_0, since the frequency of regional fires is much lower than in the dry season. Actually, when including data from the beginning of 2016, under the influence of ENSO, we observed a shift towards higher ER_{BC} in the NE directions due to the occurrence of fires in the Guyanas area. These atypical data were excluded from Fig. 6 to improve the contrast between the different air mass trajectory clusters. The NE and ENE trajectories were very similar in terms of ω_0 and ER_{BC}. Occasional dust transport events from the Sahara, mixed with BB aerosol from the Sahel region, brought aerosol particles with lower ω_0 compared to the wet season average.

The lower ER_{BC} observed in the wet season was likely due to aerosol scavenging during the transatlantic advection (Moran-Zuloaga et al., 2017), while CO is not affected by wet deposition (Liu et al., 2010). Note that ER_{BC} decreased more steeply with increasing ω_0 and their correlation was closer during the dry season (E and ESE BT clusters) in comparison to the wet season. This feature might be related to the age of the aerosol particles, because aging would make the BC become less hydrophobic (M. L. Pöhlker et al., 2017) so that it can be more efficiently removed by wet scavenging.

3.6 El Niño impact on aerosol optical properties

The aerosol optical properties measured at ATTO changed during the El Niño period at the end of 2015 and the beginning of 2016 (Fig. 3). To have a broader view on the relationships between El Niño-related

droughts conditions, increased fires abundance, and the Amazonian aerosol properties, we added scattering and absorption data from the ZF2 site published in Rizzo et al. (2013) and extended with recent data to the current ATTO time series in Fig. 7a-b. Overlapping data in 2013 (Fig. 7a and 7b) are statistically equivalent with only a few days affected by probable near-site sources. Positive Oceanic Niño Index (ONI) values (Fig. 7c) were found to be related to higher scattering and absorption coefficients in the dry season. However, the ENSO is not the only cause of precipitation anomalies in the Amazon Basin. The Atlantic Multi-Decadal Oscillation (AMO) has also been found to be causing droughts (Aragão et al., 2008). The non-ENSO daily-mean average (ZF2 and ATTO) scattering coefficient at 637 nm during the dry seasons was 24 ± 18 Mm^{-1}. This average increased up to 48 ± 33 Mm^{-1} during the ENSO periods (2009 and 2015 dry seasons). The wet season scattering coefficient average was also affected during El Niño, increasing from a non-ENSO average of 7 ± 7 Mm^{-1} to 10 ± 11 Mm^{-1} during the wet season 2016. A similar pattern was observed for $\sigma_{ap\,637}$, which increased from a non-ENSO average in the dry seasons of 3.8 ± 2.8 Mm^{-1} to an ENSO average of 5.3 ± 2.5 Mm^{-1} (2009 and 2015 dry seasons average). It is remarkable that high absorption coefficients were also measured during the dry season 2010 (5.6 ± 4.7 Mm^{-1}), a year with mostly negative ONI. However, it has been shown that an increased sea surface temperature in the Atlantic Ocean (not ENSO related) in 2010 caused a special drought period in the Amazon rain forest (Lewis et al., 2011).

3.7 Absorption wavelength dependence and BrC contribution

Open biomass burning emits a mixture of BC and OA with high absorption wavelength dependence (Andreae and Gelencsér, 2006; Hoffer et al., 2006; Kirchstetter et al., 2004). However, our observations show that sometimes LAC measured at the ATTO site can fall in the BC-only regime, with $\mathring{a}_{abs} \approx 1$. To understand this pattern, we have analyzed the relationship between the WDA and other parameters, like the OA-to-sulfate ratio and ω_0. In Fig. 8a, WDA is presented as a function of the OA-to-sulfate mass ratio. According to the result of an orthogonal fit (not shown), there is a significant correlation between these variables ($R^2 = 0.61$), and the aerosol light absorption is in the BC-only regime (shaded area in Fig. 8a) when the OA-to-sulfate ratio is lower than ~6.5, which occurred 15 % of the time in the high-absorption periods ($\sigma_{ap\,637}$ higher than the 75th percentile). On the other hand, higher OA-to-sulfate

ratios correspond to likely BrC-rich aerosol masses, which were the majority of the cases. The ω_0 at 637 nm of the BC-only regime (inter-quartile range, IQR: 0.82 – 0.86) was clearly lower than the one corresponding to the BrC-rich regime (IQR: 0.85 – 0.90).

In Fig. 8b, the BC-only regime data has been segregated by BT clusters. The air masses that are more likely to bring wavelength independent BC to the site are those with the faster wind speed: E3, E4, and ESE3. These emissions could be related to ship traffic in the Atlantic Ocean, BB in southern Africa, or power plant emissions from the west African coast. Low OA-to-sulfate ratios with high ω_0 occurred a few times and could be explained by high sulfate input from volcanic emissions in the Congo (Fioletov et al., 2016; Saturno et al., 2017a), rather than fossil fuel emissions, which are typically rich in BC.

In an effort to identify the BrC-rich trajectories, the WDA was studied for the different BT clusters that are mostly active during the dry season. Box plots corresponding to each trajectory cluster, together with the average fire counts in the geographical cluster area, are presented in Fig. 9. From the group of ESE trajectory clusters (ESE1, ESE2, and ESE3), the ESE1 trajectories exhibit the highest WDA values, with a decreasing tendency towards faster trajectories, ESE3 being the one with lowest WDA values. Even though ESE3 is the trajectory cluster with more fire counts, the fact that those fires occur farther from the ATTO site compared to the ones in the slowest trajectory, ESE1, could be related to a decrease in absorption wavelength dependence during transport. A similar pattern is observed for the easterly trajectory clusters (E1, E2, E3, and E4), where the slowest air mass trajectories comprised by the E1 cluster exhibit the highest WDA median compared to the rest of the E clusters. In the case of E4, the WDA 25th percentile is lower than the rest of the E trajectories, but it shows an increased median that can not be explained by the occurrence of fire events, which is lower than the observations for the other clusters (E2, E3, and E4). The E4 weighted fire counts are anyhow in the same order magnitude as E2 and E3 and the wavelength dependence differences could be related to different fuel types or combustion phase. Actually, the long E clusters (E3 and E4) cover more southern areas than the shorter ones (E1 and E2) and have some overlap with ESE3. By comparing grouped E and ESE clusters, it can be observed that WDA in the E clusters has higher variability compared to the ESE ones. This pattern could be associated with a wider range of sources in the E trajectories compared to ESE. The E trajectories travel over the Amazon River where ship traffic is quite significant. In fact, as can be

observed in Fig. 9, for the E3 and E4 trajectories, there is a significant amount (> 25th percentile) of measurements that fall in the BC-only regime. Something similar is only observed for the ESE3 trajectories among the ESE group. Most of the agricultural land is located along the southern margins of the Amazon rain forest (Pöhlker et al., 2018). This area is within the ESE clusters footprint. The narrower range of WDA values measured for the ESE trajectories compared to the E ones, indicates that sources in the ESE footprint are more homogeneous compared to the sources located in the E footprint. These WDA tendencies could be useful to understanding the BrC emissions and atmospheric transformations in the context of the Amazon rain forest and its surroundings.

Using the calculated BC-only WDA thresholds, we were able to estimate the BrC contribution to total absorption during the measurement period (2012 – 2017) (Fig. 10). We found that BrC contributes 24 % (IQR: 17 – 29 %) of total light absorption at 370 nm wavelength. A slight seasonal variability was observed for the BrC relative contribution, with the medians and IQR during the wet and dry season being 27 % (19 – 34) and 22 % (16 – 27), respectively. However, most of the wet season data had to be excluded, because they were from air masses rich in mineral dust, which introduces large uncertainties in the WDA method. During El Niño, at the end of 2015, open fire events were more frequent (with weighted fire counts of 1756 km^{-2} compared to the 2008 – 2016 average of 1076 km^{-2}), and the CO 95th percentile was exceeded several times. In this period, the BrC contribution had a median of 37 % (IQR: 27 – 47) and showed a significant correlation with CO (R^2 = 0.47). This significant increase of the BrC contribution could be related to the relatively short distance between the fire spots and the ATTO site. It can be observed in Fig. 10 that the El Niño influence continued during the dry season 2016 but not as strongly as in 2015. Previous observations have shown that the atmospheric lifetime of BB-emitted BrC is ~1 day due to photolysis and oxidation, which destroy the chromophores (Forrister et al., 2015; Wang et al., 2016b; Wong et al., 2017). Therefore, BrC emitted from fires in the southern borders of the Amazon rain forest, which require ~3 days to be transported to the ATTO site, is likely to be significantly photodegraded and to contribute only weakly to total aerosol light absorption after atmospheric processing.

The BC to OA mass ratio during the sampling time had a median of 0.06 (IQR: 0.04 – 0.10). The ratio BC to OA has been used before to parameterize $å_{abs}$ and ω_0 (Pokhrel et al., 2016; Saleh et al., 2014), but

little is known about this relationship for tropical forest emissions. A broader range of BC to OA mass ratio between 2014 and 2016 was observed during the dust episodes in the wet season, including those periods when regional fires were active (IQR: 0.08 – 0.24). Other periods, like the dry season, with higher BC mass concentrations, exhibited a narrower and lower BC to OA mass ratio range (IQR: 0.03 – 0.08). A scatter plot of the absorption wavelength dependence, $å_{abs}$, as a function of the BC to OA mass ratio during the North African LRT events in the wet season can be found in Fig. 11. We have found a trend where $å_{abs}$ increases with decreasing BC to OA mass ratio following an exponential function. These results are comparable to those presented by Pokhrel et al. (2016) and Saleh et al. (2014), with slightly lower $å_{abs}$ values in our study, however. This pattern could be related to a dominant presence of primary organic aerosol (POA) that has characteristically lower absorption wavelength dependence compared to SOA (Saleh et al., 2013). However, more experimental studies are required to investigate the optical properties of aerosol produced by burning different tropical forest fuels.

Summary and conclusions

This study presents the optical properties of aerosol particles at the remote ATTO site for a measurement period of 5 years (2012 – 2017). The atmospheric seasonality at ATTO strongly affects aerosol light scattering and absorption with significant increases from wet to dry season conditions due to intense biomass burning in South America and Africa. The wet season background aerosol was dominated by biogenic particles with occasional interruptions by long-range transported dust and BB aerosols from Africa to ATTO, leading to decreases in scattering Ångström exponent, $å_{sca}$, and single scattering albedo, ω_0 (637 nm). The average ω_0 during the wet season was with 0.93 ± 0.04, which is higher than the dry season average of 0.87 ± 0.03. The absorption wavelength dependence, $å_{abs}$, was relatively low with an average of 0.93 ± 0.16, and varied only slightly between seasons. The highest $å_{abs}$ were measured during BB events, but no effect on $å_{abs}$ was observed due to the presence of dust, most likely due to a size effect, given that after May 2014 absorption coefficients were measured only for sub-micron aerosol particles. The BC mass absorption coefficient (MAC) at 637 nm calculated from MAAP and SP2 measurements agrees with other studies; however, it is higher than “typical” values that

are commonly used in the literature to convert σ_{ap} into BC mass concentrations. The calculated wet season MAC average was 11.4 ± 1.2 $m^2\ g^{-1}$, and increased slightly during the dry season to an average of 12.3 ± 1.3 $m^2\ g^{-1}$ at 637 nm. These values are consistent with a strong "lensing effect" by organic coatings attached to BC aerosol particles. High OA amounts in the Amazonian atmosphere resulted in low BC to OA mass ratios, in the range of 0.04 to 0.10 (IQR). A significant correlation between BC to OA mass ratio and $\mathring{a}_{abs}$ was observed during the wet season under the influence of regional and remote BB emissions. The ΔBC/ΔCO enhancement ratios (ER_{BC}) were mostly lower than 8 ng m^{-3} ppb^{-1}, mainly due to the aging and deposition of BB aerosol particles during transport to ATTO. A higher and wider range of ER_{BC} values was observed during the dry season due to the influence of different biomass combustion phases that varied from smoldering to flaming fires.

Theoretical wavelength-dependent BC $\mathring{a}_{abs}$ were calculated and used to estimate the BrC contribution to near-UV (370 nm) light absorption. This approach resulted in medians of 27 and 22 % BrC contributions in the wet and dry season, respectively. Higher BrC contributions were measured during the El Niño period at the end of 2015 when BrC absorption at 370 nm increased to a median of 37 %. We observed that winds coming from ESE directions in the dry season were more likely to bring aerosols with a high absorption wavelength dependence, implying a higher BrC content.

In the case of prolonged drought periods in the Amazon Basin, significant increases of BrC absorption contribution could be expected due to increased fire occurrence. Long-term monitoring of light absorbing aerosol particles is required to reduce uncertainty in global climate models. The data presented here provide a contribution in this direction and can help to understand how different climatic phenomena, like El Niño, can affect the Amazon atmospheric aerosol cycling. Further investigations on the BC mixing state and morphology will be required to improve modeled calculations and BrC retrievals.

Acknowledgments

This work has been supported by the Max Planck Society (MPG) and the Paul Crutzen Graduate School (PCGS). For the operation of the ATTO site, we acknowledge the support by the German Federal Ministry of Education and Research (BMBF contract 01LB1001A) and the Brazilian Ministério da Ciência, Tecnologia e Inovação (MCTI/FINEP contract 01.11.01248.00) as well as the Amazon State

University (UEA), FAPEAM, LBA/INPA and SDS/CEUC/RDS-Uatumã. P. A. acknowledges support from FAPESP – Fundação de Amparo à Pesquisa do Estado de São Paulo. J. S. is grateful for the PhD scholarship from the Fundación Gran Mariscal de Ayacucho (Fundayacucho). This paper contains results of research conducted under the Technical/Scientific Cooperation Agreement between the National Institute for Amazonian Research, the State University of Amazonas, and the Max-Planck-Gesellschaft e.V.; the opinions expressed are the entire responsibility of the authors and not of the participating institutions. We highly acknowledge the support by the Instituto Nacional de Pesquisas da Amazônia (INPA). We would like to especially thank all the people involved in the technical, logistical, and scientific support of the ATTO project, in particular Reiner Ditz, Jürgen Kesselmeier, Alberto Quesada, Niro Higuchi, Susan Trumbore, Matthias Sörgel, Thomas Disper, Andrew Crozier, Uwe Schulz, Steffen Schmidt, Antonio Ocimar Manzi, Alcides Camargo Ribeiro, Hermes Braga Xavier, Elton Mendes da Silva, Nagib Alberto de Castro Souza, Adi Vasconcelos Brandão, Amaury Rodrigues Pereira, Antonio Huxley Melo Nascimento, Feliciano de Souza Coehlo, Thiago de Lima Xavier, Josué Ferreira de Souza, Roberta Pereira de Souza, Bruno Takeshi, and Wallace Rabelo Costa.

References

ACTRIS: ACTRIS Intercomparison Workshop for Integrating Nephelometer and Absorption Photometers, Leipzig, Germany. [online] Available from: http://www.wmo-gaw-wcc-aerosol-physics.org/files/ACTRIS-intercomparison-workshop-integrating-nephelometer-and-absorption-photometer-02-03-2013.pdf, 2014.

Ahlm, L., Nilsson, E. D., Krejci, R., Mårtensson, E. M., Vogt, M. and Artaxo, P.: Aerosol number fluxes over the Amazon rain forest during the wet season, Atmos. Chem. Phys. Discuss., 9(4), 17335–17383, doi:10.5194/acpd-9-17335-2009, 2009.

Akagi, S. K., Yokelson, R. J., Wiedinmyer, C., Alvarado, M. J., Reid, J. S., Karl, T., Crounse, J. D. and Wennberg, P. O.: Emission factors for open and domestic biomass burning for use in atmospheric models, Atmos. Chem. Phys., 11(9), 4039–4072, doi:10.5194/acp-11-4039-2011, 2011.

Anderson, T. L., Covert, D. S., Marshall, S. F., Laucks, M. L., Charlson, R. J., Waggoner, A. P., Ogren, J. A., Caldow, R., Holm, R. L., Quant, F. R., Sem, G. J., Wiedensohler, A., Ahlquist, N. A. and Bates, T. S.: Performance Characteristics of a High-Sensitivity, Three-Wavelength, Total Scatter/Backscatter Nephelometer, J. Atmos. Ocean. Technol., 13(5), 967–986, doi:10.1175/1520-0426(1996)013<0967:PCOAHS>2.0.CO;2, 1996.

Andreae, M. O.: Biomass burning: Its history, use and distribution and its impact on environmental quality and global climate, Glob. Biomass Burn. Atmos. Clim. Biosph. Implic., 15–42, 1991.

Andreae, M. O.: Raising dust in the greenhouse, Nature, 380(6573), 389–390, doi:10.1038/380389a0, 1996.

Andreae, M. O.: The dark side of aerosols, Nature, 409(6821), 671–672, doi:10.1038/35055640, 2001.

Andreae, M. O.: Aerosols before pollution, Science, 315(5808), 50–51, doi:10.1126/science.1136529, 2007.

Andreae, M. O. and Gelencsér, A.: Black carbon or brown carbon? The nature of light-absorbing carbonaceous aerosols, Atmos. Chem. Phys., 3131–3148, 2006.

Andreae, M. O. and Merlet, P.: Emission of trace gases and aerosols from biomass burning, Global Biogeochem. Cycles, 15(4), 955–966, doi:10.1029/2000GB001382, 2001.

Andreae, M. O., Browell, E. V., Garstang, M., Gregory, G. L., Harriss, R. C., Hill, G. F., Jacob, D. J., Pereira, M. C., Sachse, G. W., Setzer, A. W., Dias, P. L. S., Talbot, R. W., Torres, A. L. and Wofsy, S. C.: Biomass-burning emissions and associated haze layers over Amazonia, J. Geophys. Res., 93(D2), 1509, doi:10.1029/JD093iD02p01509, 1988.

Andreae, M. O., Anderson, B. E., Blake, D. R., Bradshaw, J. D., Collins, J. E., Gregory, G. L., Sachse, G. W. and Shipham, M. C.: Influence of plumes from biomass burning on atmospheric chemistry over the equatorial and tropical South Atlantic during CITE 3, J. Geophys. Res., 99(D6), 12793, doi:10.1029/94JD00263, 1994.

Andreae, M. O., Artaxo, P., Beck, V., Bela, M., Freitas, S., Gerbig, C., Longo, K., Munger, J. W., Wiedemann, K. T. and Wofsy, S. C.: Carbon monoxide and related trace gases and aerosols over the Amazon Basin during the wet and dry seasons, Atmos. Chem. Phys., 12(13), 6041–6065, doi:10.5194/acp-12-6041-2012, 2012.

Andreae, M. O., Acevedo, O. C., Araùjo, A., Artaxo, P., Barbosa, C. G. G., Barbosa, H. M. J., Brito, J., Carbone, S., Chi, X., Cintra, B. B. L., da Silva, N. F., Dias, N. L., Dias-Júnior, C. Q., Ditas, F., Ditz, R., Godoi, A. F. L., Godoi, R. H. M., Heimann, M., Hoffmann, T., Kesselmeier, J., Könemann, T., Krüger, M. L., Lavric, J. V, Manzi, A. O., Lopes, A. P., Martins, D. L., Mikhailov, E. F., Moran-Zuloaga, D., Nelson, B. W., Nölscher, A. C., Santos Nogueira, D., Piedade, M. T. F., Pöhlker, C., Pöschl, U., Quesada, C. A., Rizzo, L. V, Ro, C.-U., Ruckteschler, N., Sá, L. D. A., de Oliveira Sá, M., Sales, C. B., dos Santos, R. M. N., Saturno, J., Schöngart, J., Sörgel, M., de Souza, C. M., de Souza, R. A. F., Su, H., Targhetta, N., Tóta, J., Trebs, I., Trumbore, S., van Eijck, A., Walter, D., Wang, Z., Weber, B., Williams, J., Winderlich, J., Wittmann, F., Wolff, S. and Yáñez-Serrano, A. M.: The Amazon Tall Tower Observatory (ATTO): Overview of pilot measurements on ecosystem ecology, meteorology, trace gases, and aerosols, Atmos. Chem. Phys., 15(18), 10723–10776, doi:10.5194/acp-15-10723-2015, 2015.

Ångström, A.: On the Atmospheric Transmission of Sun Radiation and on Dust in the Air, Geogr. Ann., 11, 156–166 [online] Available from: http://www.jstor.org/stable/519399, 1929.

Aragão, L. E. O. ., Malhi, Y., Barbier, N., Lima, A., Shimabukuro, Y., Anderson, L. and Saatchi, S.: Interactions between rainfall, deforestation and fires during recent years in the Brazilian Amazonia, Philos. Trans. R. Soc. B Biol. Sci., 363(1498), 1779–1785, doi:10.1098/rstb.2007.0026, 2008.

Aragão, L. E. O. C., Malhi, Y., Roman-Cuesta, R. M., Saatchi, S., Anderson, L. O. and Shimabukuro, Y. E.: Spatial patterns and fire response of recent Amazonian droughts, Geophys. Res. Lett., 34(7), 1–5, doi:10.1029/2006GL028946, 2007.

Artaxo, P., Martins, J. V., Yamasoe, M. A., Procópio, A. S., Pauliquevis, T. M., Andreae, M. O., Guyon, P., Gatti, L. V. and Cordova Leal, A. M.: Physical and chemical properties of aerosols in the wet and dry seasons in Rondônia, Amazonia, J. Geophys. Res., 107(D20), 8081, doi:10.1029/2001JD000666, 2002.

Artaxo, P., Rizzo, L. V., Brito, J. F., Barbosa, H. M. J., Arana, A., Sena, E. T., Cirino, G. G., Bastos, W., Martin, S. T. and Andreae, M. O.: Atmospheric aerosols in Amazonia and land use change: from natural biogenic to biomass burning conditions, Faraday Discuss., doi:10.1039/c3fd00052d, 2013.

Barbosa, P. M., Stroppiana, D., Grégoire, J.-M. and Cardoso Pereira, J. M.: An assessment of vegetation fire in Africa (1981-1991): Burned areas, burned biomass, and atmospheric emissions, Global Biogeochem. Cycles, 13(4), 933–950, doi:10.1029/1999GB900042, 1999.

Bilbao, B. A., Leal, A. V. and Méndez, C. L.: Indigenous Use of Fire and Forest Loss in Canaima National Park, Venezuela. Assessment of and Tools for Alternative Strategies of Fire Management in Pemón Indigenous Lands, Hum. Ecol., 38(5), 663–673, doi:10.1007/s10745-010-9344-0, 2010.

Bohren, C. F. and Huffman, D. R.: Absorption and scattering of light by small particles, Wiley, Hoboken, N. J., 1983.

Bond, T. C. and Bergstrom, R. W.: Light Absorption by Carbonaceous Particles : An Investigative Review, Aerosol Sci. Technol., 40, 27–67, doi:10.1080/02786820500421521, 2006.

Bond, T. C., Streets, D. G., Yarber, K. F., Nelson, S. M., Woo, J.-H. and Klimont, Z.: A technology-based global inventory of black and organic carbon emissions from combustion, J. Geophys. Res., 109(D14), D14203, doi:10.1029/2003JD003697, 2004.

Bond, T. C., Doherty, S. J., Fahey, D. W., Forster, P. M., Berntsen, T., DeAngelo, B. J., Flanner, M. G., Ghan, S., Kärcher, B., Koch, D., Kinne, S., Kondo, Y., Quinn, P. K., Sarofim, M. C., Schultz, M. G., Schulz, M., Venkataraman, C., Zhang, H., Zhang, S., Bellouin, N., Guttikunda, S. K., Hopke, P. K., Jacobson, M. Z., Kaiser, J. W., Klimont, Z., Lohmann, U., Schwarz, J. P., Shindell, D., Storelvmo, T., Warren, S. G. and Zender, C. S.: Bounding the role of black carbon in the climate system: A scientific assessment, J. Geophys. Res. Atmos., 118(11), 5380–5552, doi:10.1002/jgrd.50171, 2013.

Brito, J., Rizzo, L. V., Morgan, W. T., Coe, H., Johnson, B., Haywood, J., Longo, K., Freitas, S., Andreae, M. O. and Artaxo, P.: Ground-based aerosol characterization during the South American Biomass Burning Analysis (SAMBBA) field experiment, Atmos. Chem. Phys., 14(22), 12069–12083, doi:10.5194/acp-14-12069-2014, 2014.

Cachier, H., Bremond, M.-P. and Buat-Ménard, P.: Determination of atmospheric soot carbon with a simple thermal method, Tellus B, 41B(3), 379–390, doi:10.1111/j.1600-0889.1989.tb00316.x, 1989.

Caponi, L., Formenti, P., Massabó, D., Di Biagio, C., Cazaunau, M., Pangui, E., Chevaillier, S., Landrot, G., Andreae, M. O., Kandler, K., Piketh, S., Saeed, T., Seibert, D., Williams, E., Balkanski, Y., Prati, P. and Doussin, J.-F.: Spectral- and size-resolved mass absorption efficiency of mineral dust aerosols in the shortwave spectrum: a simulation chamber study, Atmos. Chem. Phys., 17(11), 7175–7191, doi:10.5194/acp-17-7175-2017, 2017.

Carbone, S., Brito, J. F., Xu, L., Ng, N. L., Rizzo, L. V., Stern, R., Cirino, G. G., Holanda, B. A., Senna, E., Wolff, S., Saturno, J., Chi, X., Souza, R. A. F., Arana, A., de Sá, M., Pöhlker, M. L., Andreae, M. O., Pöhlker, C., Barbosa, H. M. J. and Artaxo, P.: Long-term chemical composition and source apportionment of submicron aerosol particles in the central Amazon basin (ATTO), Atmos. Chem. Phys. Discuss., in preparation, 2018.

Carslaw, K. S., Lee, L. A., Reddington, C. L., Pringle, K. J., Rap, A., Forster, P. M., Mann, G. W., Spracklen, D. V., Woodhouse, M. T., Regayre, L. A. and Pierce, J. R.: Large contribution of natural aerosols to uncertainty in indirect forcing, Nature, 503(7474), 67–71, doi:10.1038/nature12674, 2013.

Chand, D., Guyon, P., Artaxo, P., Schmid, O., Frank, G. P., Rizzo, L. V., Mayol-Bracero, O. L., Gatti, L. V. and Andreae, M. O.: Optical and physical properties of aerosols in the boundary layer and free troposphere over the Amazon Basin during the biomass burning season, Atmos. Chem. Phys., 6(10), 2911–2925, doi:10.5194/acp-6-2911-2006, 2006.

Chi, X., Winderlich, J., Mayer, J.-C., Panov, a. V., Heimann, M., Birmili, W., Heintzenberg, J., Cheng, Y. and Andreae, M. O.: Long-term measurements of aerosol and carbon monoxide at the ZOTTO tall tower to characterize polluted and pristine air in the Siberian taiga, Atmos. Chem. Phys., 13(24), 12271–12298, doi:10.5194/acp-13-12271-2013, 2013.

Chow, J. C., Yu, J. Z., Watson, J. G., Hang Ho, S. S., Bohannan, T. L., Hays, M. D. and Fung, K. K.: The application of thermal methods for determining chemical composition of carbonaceous aerosols: A review, J. Environ. Sci. Heal. Part A, 42(11), 1521–1541, doi:10.1080/10934520701513365, 2007.

Clarke, A. D. and Charlson, R. J.: Radiative Properties of the Background Aerosol: Absorption Component of Extinction, Science, 229(4710), 263–265, doi:10.1126/science.229.4710.263, 1985.

Cochrane, M. A.: Fire science for rainforests, Nature, 421(6926), 913–919, doi:10.1038/nature01437, 2003.

Collaud Coen, M., Weingartner, E., Apituley, A., Ceburnis, D., Fierz-Schmidhauser, R., Flentje, H., Henzing, J. S., Jennings, S. G., Moerman, M., Petzold, A., Schmid, O. and Baltensperger, U.: Minimizing light absorption measurement artifacts of

the Aethalometer: evaluation of five correction algorithms, Atmos. Meas. Tech., 3, 457–474, doi:10.5194/amt-3-457-2010, 2010.

Crutzen, P. J. and Andreae, M. O.: Biomass burning in the tropics: Impact on atmospheric chemistry and biogeochemical cycles, Science, 250(4988), 1669–1678 [online] Available from: http://www.scopus.com/inward/record.url?eid=2-s2.0-0025626194&partnerID=40&md5=8463016f82d20c79a21a47555f2811ce, 1990.

Das, S., Harshvardhan, H., Bian, H., Chin, M., Curci, G., Protonotariou, A. P., Mielonen, T., Zhang, K., Wang, H. and Liu, X.: Biomass burning aerosol transport and vertical distribution over the South African-Atlantic region, J. Geophys. Res. Atmos., 6391–6415, doi:10.1002/2016JD026421, 2017.

Davidson, E. a., de Araújo, A. C., Artaxo, P., Balch, J. K., Brown, I. F., C. Bustamante, M. M., Coe, M. T., DeFries, R. S., Keller, M., Longo, M., Munger, J. W., Schroeder, W., Soares-Filho, B. S., Souza, C. M. and Wofsy, S. C.: The Amazon basin in transition, Nature, 481(7381), 321–328, doi:10.1038/nature10717, 2012.

Denjean, C., Cassola, F., Mazzino, A., Triquet, S., Chevaillier, S., Grand, N., Bourrianne, T., Momboisse, G., Sellegri, K., Schwarzenbock, A., Freney, E., Mallet, M. and Formenti, P.: Size distribution and optical properties of mineral dust aerosols transported in the western Mediterranean, Atmos. Chem. Phys., 16(2), 1081–1104, doi:10.5194/acp-16-1081-2016, 2016.

Draxler, R. R. and Hess, G. D.: An overview of the HYSPLIT 4 modelling system for trajectories, dispersion and deposition, Aust. Met. Mag., 47(4), 295–308, 1998.

Drinovec, L., Močnik, G., Zotter, P., Prévôt, A. S. H., Ruckstuhl, C., Coz, E., Rupakheti, M., Sciare, J., Müller, T., Wiedensohler, A. and Hansen, A. D. A.: The "dual-spot" Aethalometer: an improved measurement of aerosol black carbon with real-time loading compensation, Atmos. Meas. Tech., 8(5), 1965–1979, doi:10.5194/amt-8-1965-2015, 2015.

Dubovik, O., Holben, B., Eck, T. F., Smirnov, A., Kaufman, Y. J., King, M. D., Tanré, D. and Slutsker, I.: Variability of Absorption and Optical Properties of Key Aerosol Types Observed in Worldwide Locations, J. Atmos. Sci., 59, 590–608, 2002.

Falster, D. S., Warton, D. I. and Wright, I. J.: SMATR: Standardised major axis tests and routines, ver 2.0, [online] Available from: http://www.bio.mq.edu.au/ecology/SMATR/, 2006.

Favez, O., El Haddad, I., Piot, C., Boréave, A., Abidi, E., Marchand, N., Jaffrezo, J.-L., Besombes, J.-L., Personnaz, M.-B., Sciare, J., Wortham, H., George, C. and D'Anna, B.: Inter-comparison of source apportionment models for the estimation of wood burning aerosols during wintertime in an Alpine city (Grenoble, France), Atmos. Chem. Phys., 10(12), 5295–5314, doi:10.5194/acp-10-5295-2010, 2010.

Fioletov, V. E., McLinden, C. A., Krotkov, N., Li, C., Joiner, J., Theys, N., Carn, S. and Moran, M. D.: A global catalogue of large SO2 sources and emissions derived from the Ozone Monitoring Instrument, Atmos. Chem. Phys., 16(18), 11497–11519, doi:10.5194/acp-16-11497-2016, 2016.

Fisch, G., Tota, J., Machado, L. A. T., Silva Dias, M. A. F., da F. Lyra, R. F., Nobre, C. A., Dolman, A. J. and Gash, J. H. C.: The convective boundary layer over pasture and forest in Amazonia, Theor. Appl. Climatol., 78(1–3), 47–59, doi:10.1007/s00704-004-0043-x, 2004.

Formenti, P., Andreae, M. O., Lange, L., Roberts, G., Cafmeyer, J., Rajta, I., Maenhaut, W., Holben, B. N., Artaxo, P. and Lelieveld, J.: Saharan dust in Brazil and Suriname during the Large-Scale Biosphere-Atmosphere Experiment in Amazonia

(LBA) - Cooperative LBA Regional Experiment (CLAIRE) in March 1998, J. Geophys. Res. Atmos., 106(D14), 14919–14934, doi:10.1029/2000JD900827, 2001.

Forrister, H., Liu, J., Scheuer, E., Dibb, J., Ziemba, L., Thornhill, K. L., Anderson, B., Diskin, G., Perring, A. E., Schwarz, J. P., Campuzano-Jost, P., Day, D. A., Palm, B. B., Jimenez, J. L., Nenes, A. and Weber, R. J.: Evolution of brown carbon in wildfire plumes, Geophys. Res. Lett., 42(11), 4623–4630, doi:10.1002/2015GL063897, 2015.

Fuller, K. A., Malm, W. C. and Kreidenweis, S. M.: Effects of mixing on extinction by carbonaceous particles, J. Geophys. Res. Atmos., 104(D13), 15941–15954, doi:10.1029/1998JD100069, 1999.

Fuzzi, S., Decesari, S., Facchini, M. C., Cavalli, F., Emblico, L., Mircea, M., Andreae, M. O., Trebs, I., Hoffer, A., Guyon, P., Artaxo, P., Rizzo, L. V., Lara, L. L., Pauliquevis, T., Maenhaut, W., Raes, N., Chi, X., Mayol-Bracero, O. L., Soto-García, L. L., Claeys, M., Kourtchev, I., Rissler, J., Swietlicki, E., Tagliavini, E., Schkolnik, G., Falkovich, A. H., Rudich, Y., Fisch, G. and Gatti, L. V.: Overview of the inorganic and organic composition of size-segregated aerosol in Rondônia, Brazil, from the biomass-burning period to the onset of the wet season, J. Geophys. Res. Atmos., 112(1), doi:10.1029/2005JD006741, 2007.

Garg, S., Chandra, B. P., Sinha, V., Sarda-Esteve, R., Gros, V. and Sinha, B.: Limitation of the Use of the Absorption Angstrom Exponent for Source Apportionment of Equivalent Black Carbon: a Case Study from the North West Indo-Gangetic Plain, Environ. Sci. Technol., 50(2), 814–824, doi:10.1021/acs.est.5b03868, 2016.

GES-DISC: Goddard Earth Sciences Data and Information Services Center, [online] Available from: https://giovanni.gsfc.nasa.gov/giovanni/ (Accessed 1 June 2017), 2017.

Gläser, G., Wernli, H., Kerkweg, A. and Teubler, F.: The transatlantic dust transport from North Africa to the Americas-Its characteristics and source regions, J. Geophys. Res. Atmos., 120(21), 11,231-11,252, doi:10.1002/2015JD023792, 2015.

Guyon, P., Graham, B., Beck, J., Boucher, O., Gerasopoulos, E. and Roberts, G. C.: Physical properties and concentration of aerosol particles over the Amazon tropical forest during background and biomass burning conditions, Atmos. Chem. Phys., 3, 951–967, 2003a.

Guyon, P., Boucher, O., Graham, B., Beck, J., Mayol-Bracero, O. L., Roberts, G. C., Maenhaut, W., Artaxo, P. and Andreae, M. O.: Refractive index of aerosol particles over the Amazon tropical forest during LBA-EUSTACH 1999, J. Aerosol Sci., 34(7), 883–907, doi:10.1016/S0021-8502(03)00052-1, 2003b.

Guyon, P., Graham, B., Roberts, G. C., Mayol-Bracero, O. L., Maenhaut, W., Artaxo, P. and Andreae, M. O.: Sources of optically active aerosol particles over the Amazon forest, Atmos. Environ., 38(7), 1039–1051, doi:10.1016/j.atmosenv.2003.10.051, 2004.

Guyon, P., Frank, G. P., Welling, M., Chand, D., Artaxo, P., Rizzo, L., Nishioka, G., Kolle, O., Fritsch, H., Silva Dias, M. A. F., Gatti, L. V., Cordova, A. M. and Andreae, M. O.: Airborne measurements of trace gas and aerosol particle emissions from biomass burning in Amazonia, Atmos. Chem. Phys., 5(11), 2989–3002, doi:10.5194/acp-5-2989-2005, 2005.

Gysel, M., Laborde, M., Olfert, J. S., Subramanian, R. and Gröhn, a. J.: Effective density of Aquadag and fullerene soot black carbon reference materials used for SP2 calibration, Atmos. Meas. Tech., 4(12), 2851–2858, doi:10.5194/amt-4-2851-2011, 2011.

Hamilton, D. S., Lee, L. A., Pringle, K. J., Reddington, C. L., Spracklen, D. V. and Carslaw, K. S.: Occurrence of pristine aerosol environments on a polluted planet, Proc. Natl. Acad. Sci., 111(52), 18466–18471, doi:10.1073/pnas.1415440111, 2014.

Hansen, A. D. A., Rosen, H. and Novakov, T.: The aethalometer — An instrument for the real-time measurement of optical absorption by aerosol particles, Sci. Total Environ., 36, 191–196, doi:10.1016/0048-9697(84)90265-1, 1984.

Hoffer, A., Gelencsér, A., Guyon, P., Kiss, G., Schmid, O., Frank, G. P., Artaxo, P. and Andreae, M. O.: Optical properties of humic-like substances (HULIS) in biomass-burning aerosols, Atmos. Chem. Phys., 6(11), 3563–3570, doi:10.5194/acp-6-3563-2006, 2006.

Janhäll, S., Andreae, M. O. and Pöschl, U.: Biomass burning aerosol emissions from vegetation fires: particle number and mass emission factors and size distributions, Atmos. Chem. Phys., 10(3), 1427–1439, doi:10.5194/acp-10-1427-2010, 2010.

Kirchstetter, T. W., Novakov, T. and Hobbs, P. V.: Evidence that the spectral dependence of light absorption by aerosols is affected by organic carbon, J. Geophys. Res. Atmos., 109(D21), D21208, doi:10.1029/2004JD004999, 2004.

Kondo, Y., Matsui, H., Moteki, N., Sahu, L., Takegawa, N., Kajino, M., Zhao, Y., Cubison, M. J., Jimenez, J. L., Vay, S., Diskin, G. S., Anderson, B., Wisthaler, a., Mikoviny, T., Fuelberg, H. E., Blake, D. R., Huey, G., Weinheimer, a. J., Knapp, D. J. and Brune, W. H.: Emissions of black carbon, organic, and inorganic aerosols from biomass burning in North America and Asia in 2008, J. Geophys. Res., 116(D8), D08204, doi:10.1029/2010JD015152, 2011.

Laborde, M., Crippa, M., Tritscher, T., Jurányi, Z., Decarlo, P. F., Temime-Roussel, B., Marchand, N., Eckhardt, S., Stohl, A., Baltensperger, U., Prévôt, a. S. H., Weingartner, E. and Gysel, M.: Black carbon physical properties and mixing state in the European megacity Paris, Atmos. Chem. Phys., 13(11), 5831–5856, doi:10.5194/acp-13-5831-2013, 2013.

Lack, D. a., Bahreni, R., Langridge, J. M., Gilman, J. B. and Middlebrook, a. M.: Brown carbon absorption linked to organic mass tracers in biomass burning particles, Atmos. Chem. Phys., 13(5), 2415–2422, doi:10.5194/acp-13-2415-2013, 2013.

Lack, D. A. and Langridge, J. M.: On the attribution of black and brown carbon light absorption using the Ångström exponent, Atmos. Chem. Phys., 13(20), 10535–10543, doi:10.5194/acp-13-10535-2013, 2013.

Lack, D. A., Cappa, C. D., Covert, D. S., Baynard, T., Massoli, P., Sierau, B., Bates, T. S., Quinn, P. K., Lovejoy, E. R. and Ravishankara, A. R.: Bias in Filter-Based Aerosol Light Absorption Measurements Due to Organic Aerosol Loading: Evidence from Ambient Measurements, Aerosol Sci. Technol., 42(12), 1033–1041, doi:10.1080/02786820802389277, 2008.

Laskin, A., Laskin, J. and Nizkorodov, S. A.: Chemistry of Atmospheric Brown Carbon, Chem. Rev., 115(10), 4335–4382, doi:10.1021/cr5006167, 2015.

Lewis, K., Arnott, W. P., Moosmüller, H. and Wold, C. E.: Strong spectral variation of biomass smoke light absorption and single scattering albedo observed with a novel dual-wavelength photoacoustic instrument, J. Geophys. Res., 113(D16), D16203, doi:10.1029/2007JD009699, 2008.

Lewis, S. L., Brando, P. M., Phillips, O. L., van der Heijden, G. M. F. and Nepstad, D.: The 2010 Amazon Drought, Science, 331(6017), 554–554, doi:10.1126/science.1200807, 2011.

Liu, D., Flynn, M., Gysel, M., Targino, A., Crawford, I., Bower, K., Choularton, T., Jurányi, Z., Steinbacher, M., Hüglin, C., Curtius, J., Kampus, M., Petzold, A., Weingartner, E., Baltensperger, U. and Coe, H.: Single particle characterization of

black carbon aerosols at a tropospheric alpine site in Switzerland, Atmos. Chem. Phys., 10(15), 7389–7407, doi:10.5194/acp-10-7389-2010, 2010.

Liu, D., Taylor, J. W., Young, D. E., Flynn, M. J., Coe, H. and Allan, J. D.: The effect of complex black carbon microphysics on the determination of the optical properties of brown carbon, Geophys. Res. Lett., 42(2), 613–619, doi:10.1002/2014GL062443, 2015.

Liu, D., Whitehead, J., Alfarra, M. R., Reyes-Villegas, E., Spracklen, D. V., Reddington, C. L., Kong, S., Williams, P. I., Ting, Y.-C., Haslett, S., Taylor, J. W., Flynn, M. J., Morgan, W. T., McFiggans, G., Coe, H. and Allan, J. D.: Black-carbon absorption enhancement in the atmosphere determined by particle mixing state, Nat. Geosci., 10(3), 184–188, doi:10.1038/ngeo2901, 2017.

Martin, S. T., Andreae, M. O., Althausen, D., Artaxo, P., Baars, H., Borrmann, S., Chen, Q., Farmer, D. K., Guenther, A., Gunthe, S. S., Jimenez, J. L., Karl, T., Longo, K., Manzi, A., Müller, T., Pauliquevis, T., Petters, M. D., Prenni, A. J., Pöschl, U., Rizzo, L. V., Schneider, J., Smith, J. N., Swietlicki, E., Tota, J., Wang, J., Wiedensohler, A. and Zorn, S. R.: An overview of the Amazonian Aerosol Characterization Experiment 2008 (AMAZE-08), Atmos. Chem. Phys., 10(23), 11415–11438, doi:10.5194/acp-10-11415-2010, 2010a.

Martin, S. T., Andreae, M. O., Artaxo, P., Baumgardner, D., Chen, Q., Goldstein, A. H., Guenther, A., Heald, C. L., Mayol-Bracero, O. L., McMurry, P. H., Pauliquevis, T., Pöschl, U., Prather, K. A., Roberts, G. C., Saleska, S. R., Silva Dias, M. A., Spracklen, D. V., Swietlicki, E. and Trebs, I.: Sources and properties of Amazonian aerosol particles, Rev. Geophys., 48(2), RG2002, doi:10.1029/2008RG000280, 2010b.

Martin, S. T., Artaxo, P., Machado, L. A. T., Manzi, A. O., Souza, R. A. F., Schumacher, C., Wang, J., Andreae, M. O., Barbosa, H. M. J., Fan, J., Fisch, G., Goldstein, A. H., Guenther, A., Jimenez, J. L., Pöschl, U., Silva Dias, M. A., Smith, J. N. and Wendisch, M.: Introduction: Observations and Modeling of the Green Ocean Amazon (GoAmazon2014/5), Atmos. Chem. Phys., 16(8), 4785–4797, doi:10.5194/acp-16-4785-2016, 2016.

Martin, S. T., Artaxo, P., Machado, L., Manzi, A. O., Souza, R. A. F., Schumacher, C., Wang, J., Biscaro, T., Brito, J., Calheiros, A., Jardine, K., Medeiros, A., Portela, B., de Sá, S. S., Adachi, K., Aiken, A. C., Albrecht, R., Alexander, L., Andreae, M. O., Barbosa, H. M. J., Buseck, P., Chand, D., Comstock, J. M., Day, D. A., Dubey, M., Fan, J., Fast, J., Fisch, G., Fortner, E., Giangrande, S., Gilles, M., Goldstein, A. H., Guenther, A., Hubbe, J., Jensen, M., Jimenez, J. L., Keutsch, F. N., Kim, S., Kuang, C., Laskin, A., McKinney, K., Mei, F., Miller, M., Nascimento, R., Pauliquevis, T., Pekour, M., Peres, J., Petäjä, T., Pöhlker, C., Pöschl, U., Rizzo, L., Schmid, B., Shilling, J. E., Dias, M. A. S., Smith, J. N., Tomlinson, J. M., Tóta, J. and Wendisch, M.: The Green Ocean Amazon Experiment (GoAmazon2014/5) Observes Pollution Affecting Gases, Aerosols, Clouds, and Rainfall over the Rain Forest, Bull. Am. Meteorol. Soc., 98(5), 981–997, doi:10.1175/BAMS-D-15-00221.1, 2017.

Massabò, D., Caponi, L., Bernardoni, V., Bove, M. C., Brotto, P., Calzolai, G., Cassola, F., Chiari, M., Fedi, M. E., Fermo, P., Giannoni, M., Lucarelli, F., Nava, S., Piazzalunga, A., Valli, G., Vecchi, R. and Prati, P.: Multi-wavelength optical determination of black and brown carbon in atmospheric aerosols, Atmos. Environ., 108, 1–12, doi:10.1016/j.atmosenv.2015.02.058, 2015.

Mikhailov, E., Mironova, S., Mironov, G., Vlasenko, S., Panov, A., Chi, X., Walter, D., Carbone, S., Artaxo, P., Pöschl, U. and Andreae, M.: Long-term measurements (2010-2014) of carbonaceous aerosol and carbon monoxide at the Zotino Tall

Tower Observatory (ZOTTO) in central Siberia, Atmos. Chem. Phys. Discuss., (May), 1–60, doi:10.5194/acp-2017-409, 2017.

Mishchenko, M. I., Dlugach, J. M., Yanovitskij, E. G. and Zakharova, N. T.: Bidirectional reflectance of flat, optically thick particulate layers: an efficient radiative transfer solution and applications to snow and soil surfaces, J. Quant. Spectrosc. Radiat. Transf., 63(2–6), 409–432, doi:10.1016/S0022-4073(99)00028-X, 1999.

Moosmüller, H., Chakrabarty, R. K., Ehlers, K. M. and Arnott, W. P.: Absorption Ångström coefficient, brown carbon, and aerosols: basic concepts, bulk matter, and spherical particles, Atmos. Chem. Phys., 11(3), 1217–1225, doi:10.5194/acp-11-1217-2011, 2011.

Moran-Zuloaga, D., Ditas, F., Walter, D., Saturno, J., Brito, J., Carbone, S., Chi, X., Hrabě de Angelis, I., Baars, H., Godoi, R. H. M., Heese, B., Holanda, B. A., Lavrič, J. V., Martin, S. T., Ming, J., Pöhlker, M., Ruckteschler, N., Su, H., Wang, Y., Wang, Q., Wang, Z., Weber, B., Wolff, S., Artaxo, P., Pöschl, U., Andreae, M. O. and Pöhlker, C.: Long-term study on coarse mode aerosols in the Amazon rain forest with the frequent intrusion of Saharan dust plumes, Atmos. Chem. Phys. Discuss., 1–52, doi:10.5194/acp-2017-1043, 2017.

Moteki, N. and Kondo, Y.: Method to measure time-dependent scattering cross sections of particles evaporating in a laser beam, J. Aerosol Sci., 39(4), 348–364, doi:10.1016/j.jaerosci.2007.12.002, 2008.

Müller, T., Henzing, J. S., de Leeuw, G., Wiedensohler, A., Alastuey, A., Angelov, H., Bizjak, M., Collaud Coen, M., Engström, J. E., Gruening, C., Hillamo, R., Hoffer, A., Imre, K., Ivanow, P., Jennings, G., Sun, J. Y., Kalivitis, N., Karlsson, H., Komppula, M., Laj, P., Li, S.-M., Lunder, C., Marinoni, A., Martins dos Santos, S., Moerman, M., Nowak, A., Ogren, J. a., Petzold, A., Pichon, J. M., Rodriquez, S., Sharma, S., Sheridan, P. J., Teinilä, K., Tuch, T., Viana, M., Virkkula, A., Weingartner, E., Wilhelm, R. and Wang, Y. Q.: Characterization and intercomparison of aerosol absorption photometers: result of two intercomparison workshops, Atmos. Meas. Tech., 4(2), 245–268, doi:10.5194/amt-4-245-2011, 2011a.

Müller, T., Laborde, M., Kassell, G. and Wiedensohler, A.: Design and performance of a three-wavelength LED-based total scatter and backscatter integrating nephelometer, Atmos. Meas. Tech., 4(6), 1291–1303, doi:10.5194/amt-4-1291-2011, 2011b.

Nepstad, D. C., Stickler, C. M., Filho, B. S.- and Merry, F.: Interactions among Amazon land use, forests and climate: prospects for a near-term forest tipping point., Philos. Trans. R. Soc. Lond. B. Biol. Sci., 363(1498), 1737–1746, doi:10.1098/rstb.2007.0036, 2008.

Ng, N. L., Herndon, S. C., Trimborn, A., Canagaratna, M. R., Croteau, P. L., Onasch, T. B., Sueper, D., Worsnop, D. R., Zhang, Q., Sun, Y. L. and Jayne, J. T.: An Aerosol Chemical Speciation Monitor (ACSM) for Routine Monitoring of the Composition and Mass Concentrations of Ambient Aerosol, Aerosol Sci. Technol., 45(7), 780–794, doi:10.1080/02786826.2011.560211, 2011.

Petzold, A. and Schönlinner, M.: Multi-angle absorption photometry—a new method for the measurement of aerosol light absorption and atmospheric black carbon, J. Aerosol Sci., 35(4), 421–441, doi:10.1016/j.jaerosci.2003.09.005, 2004.

Petzold, a., Ogren, J. a., Fiebig, M., Laj, P., Li, S.-M., Baltensperger, U., Holzer-Popp, T., Kinne, S., Pappalardo, G., Sugimoto, N., Wehrli, C., Wiedensohler, a. and Zhang, X.-Y.: Recommendations for reporting "black carbon" measurements, Atmos. Chem. Phys., 13(16), 8365–8379, doi:10.5194/acp-13-8365-2013, 2013.

Pöhlker, C., Saturno, J., Krüger, M. L., Förster, J.-D., Weigand, M., Wiedemann, K. T., Bechtel, M., Artaxo, P. and Andreae, M. O.: Efflorescence upon humidification? X-ray microspectroscopic in-situ observation of changes in aerosol microstructure and phase state upon hydration, Geophys. Res. Lett., 41, 3681–3689, doi:10.1002/2014GL059409, 2014.

Pöhlker, C., Walter, D., Paulsen, H., Könemann, T., Moran-Zuloaga, D., Pickersgill, D., Ditas, F., Saturno, J., Lammel, G., Després, V. R., Artaxo, P. and Andreae, M. O.: Land cover and its transformation in the backward trajectory footprint region of the Amazon Tall Tower Observatory, Atmos. Chem. Phys. Discuss., submitted, 2018.

Pöhlker, M. L., Ditas, F., Saturno, J., Klimach, T., Hrabě de Angelis, I., Araùjo, A., Brito, J., Carbone, S., Cheng, Y., Chi, X., Ditz, R., Gunthe, S. S., Kandler, K., Kesselmeier, J., Könemann, T., Lavrič, J. V., Martin, S. T., Mikhailov, E., Moran-Zuloaga, D., Rizzo, L. V., Rose, D., Su, H., Thalman, R., Walter, D., Wang, J., Wolff, S., Barbosa, H. M. J., Artaxo, P., Andreae, M. O., Pöschl, U. and Pöhlker, C.: Long-term observations of cloud condensation nuclei in the Amazon rain forest - Part 2: Variability and characteristic differences under near-pristine, biomass burning, and long-range transport conditions, Atmos. Chem. Phys. Discuss., 1–51, doi:10.5194/acp-2017-847, 2017.

Pokhrel, R. P., Wagner, N. L., Langridge, J. M., Lack, D. A., Jayarathne, T., Stone, E. A., Stockwell, C. E., Yokelson, R. J. and Murphy, S. M.: Parameterization of single-scattering albedo (SSA) and absorption Ångström exponent (AAE) with EC / OC for aerosol emissions from biomass burning, Atmos. Chem. Phys., 16(15), 9549–9561, doi:10.5194/acp-16-9549-2016, 2016.

Pöschl, U., Martin, S. T., Sinha, B., Chen, Q., Gunthe, S. S., Huffman, J. A., Borrmann, S., Farmer, D. K., Garland, R. M., Helas, G., Jimenez, J. L., King, S. M., Manzi, A., Mikhailov, E., Pauliquevis, T., Petters, M. D., Prenni, A. J., Roldin, P., Rose, D., Schneider, J., Su, H., Zorn, S. R., Artaxo, P. and Andreae, M. O.: Rainforest Aerosols as Biogenic Nuclei of Clouds and Precipitation in the Amazon, Science, 329(5998), 1513–1516, doi:10.1126/science.1191056, 2010.

Prospero, J. M., Glaccum, R. A. and Nees, R. T.: Atmospheric transport of soil dust from Africa to South America, Nature, 289(5798), 570–572, doi:10.1038/289570a0, 1981.

Raatikainen, T., Brus, D., Hyvärinen, A.-P., Svensson, J., Asmi, E. and Lihavainen, H.: Black carbon concentrations and mixing state in the Finnish Arctic, Atmos. Chem. Phys., 15(11), 10057–10070, doi:10.5194/acpd-15-15621-2015, 2015.

R Development Core Team: R: A language and environment for statistical computing, [online] Available from: http://www.r-project.org, 2009.

Reid, J. S., Hobbs, P. V, Ferek, R. J., Blake, D. R., Martins, J. V., Dunlap, M. R. and Liousse, C.: Physical, chemical, and optical properties of regional hazes dominated by smoke in Brazil, J. Geophys. Res. Atmos., 103(D24), 32059–32080, doi:10.1029/98JD00458, 1998.

Reid, J. S., Eck, T. F., Christopher, S. a., Koppmann, R., Dubovik, O., Eleuterio, D. P., Holben, B. N., Reid, E. a. and Zhang, J.: A review of biomass burning emissions part III: intensive optical properties of biomass burning particles, Atmos. Chem. Phys., 5, 827–849, doi:10.5194/acpd-4-5201-2004, 2005.

Ridley, D. a., Heald, C. L. and Prospero, J. M.: What controls the recent changes in African mineral dust aerosol across the Atlantic?, Atmos. Chem. Phys., 14(11), 5735–5747, doi:10.5194/acp-14-5735-2014, 2014.

Rincón, A. G., Guzmán, M. I., Hoffmann, M. R. and Colussi, A. J.: Thermochromism of Model Organic Aerosol Matter, J. Phys. Chem. Lett., 1(1), 368–373, doi:10.1021/jz900186e, 2010.

Rizzo, L. V., Correia, A. L., Artaxo, P., Procópio, A. S. and Andreae, M. O.: Spectral dependence of aerosol light absorption over the Amazon Basin, Atmos. Chem. Phys., 11, 8899–8912, doi:10.5194/acp-11-8899-2011, 2011.

Rizzo, L. V., Artaxo, P., Müller, T., Wiedensohler, A., Paixão, M., Cirino, G. G., Arana, A., Swietlicki, E., Roldin, P., Fors, E. O., Wiedemann, K. T., Leal, L. S. M. and Kulmala, M.: Long term measurements of aerosol optical properties at a primary forest site in Amazonia, Atmos. Chem. Phys., 13, 2391–2413, doi:10.5194/acp-13-2391-2013, 2013.

Roberts, G. C., Nenes, A., Seinfeld, J. H. and Andreae, M. O.: Impact of biomass burning on cloud properties in the Amazon Basin, J. Geophys. Res., 108(D2), 4062, doi:10.1029/2001JD000985, 2003.

Saleh, R., Hennigan, C. J., McMeeking, G. R., Chuang, W. K., Robinson, E. S., Coe, H., Donahue, N. M. and Robinson, a. L.: Absorptivity of brown carbon in fresh and photo-chemically aged biomass-burning emissions, Atmos. Chem. Phys., 13(15), 7683–7693, doi:10.5194/acp-13-7683-2013, 2013.

Saleh, R., Robinson, E. S., Tkacik, D. S., Ahern, A. T., Liu, S., Aiken, A. C., Sullivan, R. C., Presto, A. a, Dubey, M. K., Yokelson, R. J., Donahue, N. M. and Robinson, A. L.: Brownness of organics in aerosols from biomass burning linked to their black carbon content, Nat. Geosci., 7(August), 2–5, doi:10.1038/ngeo2220, 2014.

Salvador, P., Almeida, S. M., Cardoso, J., Almeida-Silva, M., Nunes, T., Cerqueira, M., Alves, C., Reis, M. A., Chaves, P. C., Artíñano, B. and Pio, C.: Composition and origin of PM10 in Cape Verde: Characterization of long-range transport episodes, Atmos. Environ., 127, 326–339, doi:10.1016/j.atmosenv.2015.12.057, 2016.

Sandradewi, J., Prévôt, A. S. H., Szidat, S., Perron, N., Alfarra, M. R., Lanz, V. a, Weingartner, E. and Baltensperger, U.: Using aerosol light absorption measurements for the quantitative determination of wood burning and traffic emission contributions to particulate matter., Environ. Sci. Technol., 42(9), 3316–23 [online] Available from: http://www.ncbi.nlm.nih.gov/pubmed/18522112, 2008.

Saturno, J., Ditas, F., Penning de Vries, M., Holanda, B. A., Pöhlker, M. L., Carbone, S., Walter, D., Bobrowski, N., Brito, J., Chi, X., Dinger, F., Gutmann, A., Hrabe de Angelis, I., Machado, L. A. T., Moran-Zuloaga, D., Rüdiger, J., Schneider, J., Schulz, C., Wang, Q., Wendisch, M., Artaxo, P., Wagner, T., Pöschl, U., Andreae, M. O. and Pöhlker, C.: African volcanic emissions influencing atmospheric aerosol particles over the Amazon rain forest, Atmos. Chem. Phys. Discuss., https://doi.org/10.5194/acp-2017-1152, in review, 2017a.

Saturno, J., Pöhlker, C., Massabò, D., Brito, J., Carbone, S., Cheng, Y., Chi, X., Ditas, F., Hrabě de Angelis, I., Morán-Zuloaga, D., Pöhlker, M. L., Rizzo, L. V, Walter, D., Wang, Q., Artaxo, P., Prati, P. and Andreae, M. O.: Comparison of different Aethalometer correction schemes and a reference multi-wavelength absorption technique for ambient aerosol data, Atmos. Meas. Tech., 10(8), 2837–2850, doi:10.5194/amt-10-2837-2017, 2017b.

Schkolnik, G., Chand, D., Hoffer, A., Andreae, M. O., Erlick, C., Swietlicki, E. and Rudich, Y.: Constraining the density and complex refractive index of elemental and organic carbon in biomass burning aerosol using optical and chemical measurements, Atmos. Environ., 41(5), 1107–1118, doi:10.1016/j.atmosenv.2006.09.035, 2007.

Schuster, G. L., Dubovik, O., Arola, A., Eck, T. F. and Holben, B. N.: Remote sensing of soot carbon – Part 2: Understanding the absorption Ångström exponent, Atmos. Chem. Phys., 16(3), 1587–1602, doi:10.5194/acp-16-1587-2016, 2016.

Schwarz, J. P., Gao, R. S., Fahey, D. W., Thomson, D. S., Watts, L. A., Wilson, J. C., Reeves, J. M., Darbeheshti, M., Baumgardner, D. G., Kok, G. L., Chung, S. H., Schulz, M., Hendricks, J., Lauer, A., Kärcher, B., Slowik, J. G., Rosenlof, K. H., Thompson, T. L., Langford, A. O., Loewenstein, M. and Aikin, K. C.: Single-particle measurements of midlatitude black carbon and light-scattering aerosols from the boundary layer to the lower stratosphere, J. Geophys. Res., 111(D16), D16207, doi:10.1029/2006JD007076, 2006.

Seinfeld, J. H., Bretherton, C., Carslaw, K. S., Coe, H., DeMott, P. J., Dunlea, E. J., Feingold, G., Ghan, S., Guenther, A. B., Kahn, R., Kraucunas, I., Kreidenweis, S. M., Molina, M. J., Nenes, A., Penner, J. E., Prather, K. A., Ramanathan, V., Ramaswamy, V., Rasch, P. J., Ravishankara, A. R., Rosenfeld, D., Stephens, G. and Wood, R.: Improving our fundamental understanding of the role of aerosol−cloud interactions in the climate system, Proc. Natl. Acad. Sci., 113(21), 5781–5790, doi:10.1073/pnas.1514043113, 2016.

Snelling, D. R., Smallwood, G. J., Liu, F., Gülder, Ö. L. and Bachalo, W. D.: A calibration-independent laser-induced incandescence technique for soot measurement by detecting absolute light intensity, Appl. Opt., 44(31), 6773, doi:10.1364/AO.44.006773, 2005.

Stephens, M., Turner, N. and Sandberg, J.: Particle Identification by Laser-Induced Incandescence in a Solid-State Laser Cavity, Appl. Opt., 42(19), 3726, doi:10.1364/AO.42.003726, 2003.

Stull, R. B.: An Introduction to Boundary Layer Meteorology, Springer Netherlands., 1988.

Subramanian, R., Kok, G. L., Baumgardner, D., Clarke, A., Shinozuka, Y., Campos, T. L., Heizer, C. G., Stephens, B. B., de Foy, B., Voss, P. B. and Zaveri, R. A.: Black carbon over Mexico: the effect of atmospheric transport on mixing state, mass absorption cross-section, and BC/CO ratios, Atmos. Chem. Phys., 10(1), 219–237, doi:10.5194/acp-10-219-2010, 2010.

Sumlin, B. J., Pandey, A., Walker, M. J., Pattison, R. S., Williams, B. J. and Chakrabarty, R. K.: Atmospheric Photooxidation Diminishes Light Absorption by Primary Brown Carbon Aerosol from Biomass Burning, Environ. Sci. Technol. Lett., 4(12), 540–545, doi:10.1021/acs.estlett.7b00393, 2017.

Talbot, R. W., Andreae, M. O., Berresheim, H., Artaxo, P., Garstang, M., Harriss, R. C., Beecher, K. M. and Li, S. M.: Aerosol chemistry during the wet season in central Amazonia: The influence of long-range transport, J. Geophys. Res., 95(D10), 16955, doi:10.1029/JD095iD10p16955, 1990.

Tasoglou, A., Saliba, G., Subramanian, R. and Pandis, S. N.: Absorption of chemically aged biomass burning carbonaceous aerosol, J. Aerosol Sci., 113, 141–152, doi:10.1016/j.jaerosci.2017.07.011, 2017.

Tuch, T. M., Haudek, A., Müller, T., Nowak, A., Wex, H. and Wiedensohler, A.: Design and performance of an automatic regenerating adsorption aerosol dryer for continuous operation at monitoring sites, Atmos. Meas. Tech., 2(2), 417–422, doi:10.5194/amt-2-417-2009, 2009.

Virkkula, A., Backman, J., Aalto, P. P., Hulkkonen, M., Riuttanen, L., Nieminen, T., Dal Maso, M., Sogacheva, L., De Leeuw, G. and Kulmala, M.: Seasonal cycle, size dependencies, and source analyses of aerosol optical properties at the SMEAR II measurement station in Hyytiälä, Finland, Atmos. Chem. Phys., 11(9), 4445–4468, doi:10.5194/acp-11-4445-2011, 2011.

Wang, Q., Huang, R.-J., Cao, J., Han, Y., Wang, G., Li, G., Wang, Y., Dai, W., Zhang, R. and Zhou, Y.: Mixing State of Black Carbon Aerosol in a Heavily Polluted Urban Area of China: Implications for Light Absorption Enhancement, Aerosol Sci. Technol., 48(7), 689–697, doi:10.1080/02786826.2014.917758, 2014.

Wang, Q., Saturno, J., Chi, X., Walter, D., Lavric, J. V., Moran-Zuloaga, D., Ditas, F., Pöhlker, C., Brito, J., Carbone, S., Artaxo, P. and Andreae, M. O.: Modeling investigation of light-absorbing aerosols in the Amazon Basin during the wet season, Atmos. Chem. Phys., 16(22), 14775–14794, doi:10.5194/acp-16-14775-2016, 2016a.

Wang, X., Heald, C. L., Sedlacek, A. J., de Sá, S. S., Martin, S. T., Alexander, M. L., Watson, T. B., Aiken, A. C., Springston, S. R. and Artaxo, P.: Deriving brown carbon from multiwavelength absorption measurements: method and application to AERONET and Aethalometer observations, Atmos. Chem. Phys., 16(19), 12733–12752, doi:10.5194/acp-16-12733-2016, 2016b.

Warton, D. I., Wright, I. J., Falster, D. S. and Westoby, M.: Bivariate line-fitting methods for allometry., Biol. Rev. Camb. Philos. Soc., 81(2), 259–91, doi:10.1017/S1464793106007007, 2006.

Weingartner, E., Saathoff, H., Schnaiter, M., Streit, N., Bitnar, B. and Baltensperger, U.: Absorption of light by soot particles: determination of the absorption coefficient by means of aethalometers, J. Aerosol Sci., 34(10), 1445–1463, doi:10.1016/S0021-8502(03)00359-8, 2003.

Winderlich, J., Chen, H., Gerbig, C., Seifert, T., Kolle, O., Lavrič, J. V., Kaiser, C., Höfer, A. and Heimann, M.: Continuous low-maintenance CO_2/CH_4/H_2O measurements at the Zotino Tall Tower Observatory (ZOTTO) in Central Siberia, Atmos. Meas. Tech., 3(4), 1113–1128, doi:10.5194/amt-3-1113-2010, 2010.

Womack, C., Manfred, K., Wagner, N., He, Q., Rudich, Y., Brown, S. and Washenfelder, R.: Characterizing the optical properties of brown carbon aerosol from biomass burning using broadband cavity enhanced spectroscopy, in Atmospheric Chemistry Gordon Research Conference., 2017.

Wong, J. P. S., Nenes, A. and Weber, R. J.: Changes in Light Absorptivity of Molecular Weight Separated Brown Carbon Due to Photolytic Aging, Environ. Sci. Technol., 51(15), 8414–8421, doi:10.1021/acs.est.7b01739, 2017.

Zanatta, M., Gysel, M., Bukowiecki, N., Müller, T., Weingartner, E., Areskoug, H., Fiebig, M., Yttri, K. E., Mihalopoulos, N., Kouvarakis, G., Beddows, D., Harrison, R. M., Cavalli, F., Putaud, J. P., Spindler, G., Wiedensohler, A., Alastuey, A., Pandolfi, M., Sellegri, K., Swietlicki, E., Jaffrezo, J. L., Baltensperger, U. and Laj, P.: A European aerosol phenomenology-5: Climatology of black carbon optical properties at 9 regional background sites across Europe, Atmos. Environ., 145, 346–364, doi:10.1016/j.atmosenv.2016.09.035, 2016.

Table A1. List of frequently used symbols and acronyms

Description	Acronym	Symbol	Units
Black carbon	BC		
Brown carbon	BrC		
Equivalent black carbon	BC_e		
Refractory black carbon	rBC		
Organic carbon	OC		
Organic aerosol	OA		
Light-absorbing carbonaceous matter	LAC		
ΔBC/ΔCO enhancement ratio	ER_{BC}		
Attenuation coefficient	ATN	σ_{ATN}	m^{-1}
Absorption coefficient		σ_{ap}	m^{-1}
Scattering coefficient		σ_{sp}	m^{-1}
Absorption Ångström exponent	AAE	$\mathring{a}_{abs}$	
Scattering Ångström exponent	SAE	$\mathring{a}_{sca}$	
Wavelength dependence of $\mathring{a}_{abs}$	WDA		
Mass attenuation cross-section		α_{atn}	$m^2\,g^{-1}$
(BC) Mass absorption cross-section	MAC	α_{abs}	$m^2\,g^{-1}$
Backscattering coefficient		σ_{bsp}	m^{-1}
Single scattering albedo	SSA	ω_0	
Aerosol optical depth	AOD		
Condensation nuclei number concentration (> 10 nm)		N_{CN}	cm^{-3}
Accumulation mode particle number concentration (100 to 430 nm)		N_{acc}	cm^{-3}
Precipitation at ATTO region of interest (ROI), Fig. 1a		P_{ATTO}	mm
Equivalent potential temperature		θ_e	K
Amazon Tall Tower Observatory	ATTO		
Backward trajectory	BT		
Long-range transport	LRT		
El Niño Southern Oscillation	ENSO		
Oceanic Niño Index	ONI		
Biomass burning	BB		
Fossil fuel	FF		
Coordinated universal time	UTC		
Local time	LT		
Inter-quartile range	IQR		
Domain of interest, Fig. 2a	DOI		

Table 1. Descriptive statistics (mean ± standard deviation and interquartile range, IQR) of daily-averaged aerosol optical properties over the Amazon rain forest during the different seasons and the entire measurement period.

	Wavelength	Wet season (Feb – Mar – Apr – May)		Dry season (Aug – Sep – Oct – Nov)		Entire period (2012 – 2017)	
		Mean ± SD	IQR	Mean ± SD	IQR	Mean ± SD	IQR
Scattering coefficient σ_{sp} [Mm^{-1}]	450 nm	9 ± 11	(5.1 – 11)	47 ± 35	(24 – 64)	31 ± 35	(10 – 39)
	550 nm	7.5 ± 9.3	(3.8 – 8.7)	33 ± 25	(17 – 46)	22 ± 25	(7 – 28)
	637 nm	6.4 ± 8.9	(3.0 – 7.4)	26 ± 19	(13 – 35)	17 ± 19	(6 – 23)
Absorption coefficient σ_{ap} [Mm^{-1}]	637 nm	0.68 ± 0.91	(0.17 – 0.72)	4.0 ± 2.2	(2.4 – 5.1)	2.1 ± 2.2	(0.43 – 3.2)
Single scattering albedo ω_0	637 nm	0.93 ± 0.04	(0.91 – 0.96)	0.87 ± 0.03	(0.84 – 0.89)	0.89 ± 0.04	(0.86 – 0.93)
Scattering Ångström exp. * $å_{sca}$		1.29 ± 0.50	(0.98 – 1.65)	1.71 ± 0.24	(1.53 – 1.89)	1.54 ± 0.42	(1.32 – 1.84)
Absorption Ångström exp. * $å_{abs}$		0.91 ± 0.19	(0.80 – 0.98)	0.94 ± 0.16	(0.84 – 1.03)	0.93 ± 0.16	(0.83 – 1.01)
Mass absorption cross-section α_{abs} [$m^2\ g^{-1}$] **	637 nm	11.4 ± 1.2	(10.8 – 12.0)	12.3 ± 1.3 [a]	(11.4 – 13.3) [a]	11.9 ± 1.4	(11.0 – 13.0)

* Calculated by applying a log-log linear fit to measurements at all available wavelengths.
** Calculated by fitting 8-channel SP2 and MAAP data.
[a] Including data from July 2015/16 (wet-to-dry transition season).

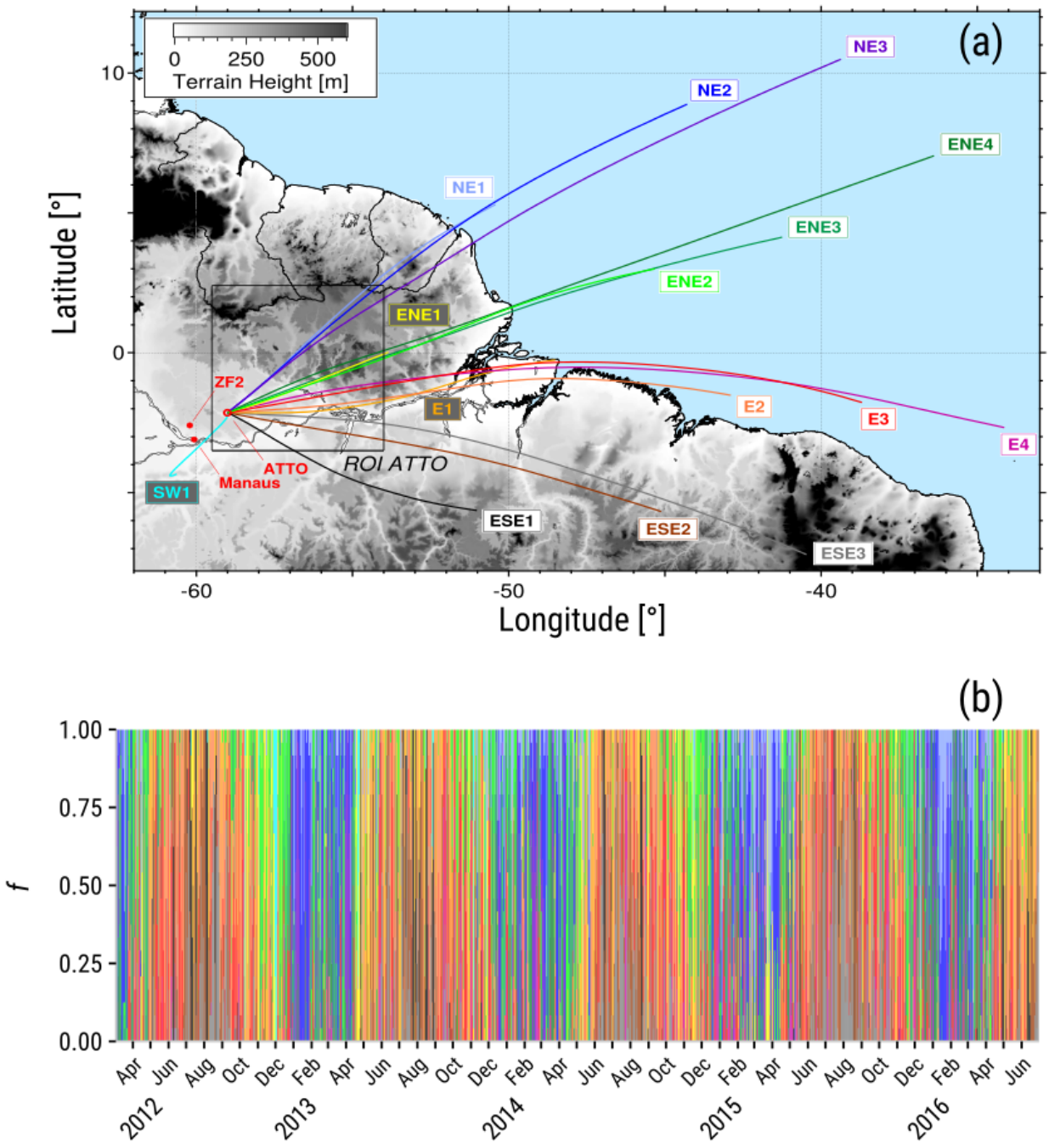

Figure 1. (a) Map of the northeastern Amazon Basin including averaged backward trajectory clusters and the region of interest (ROI) (59° W to 54° W; 3.5° S to 2.4° N), as a black rectangle, used to retrieve precipitation in the ATTO area. (b) Time series of the frequency of occurrence of each BT cluster during the sampling period. Adapted from Pöhlker et al. (2018).

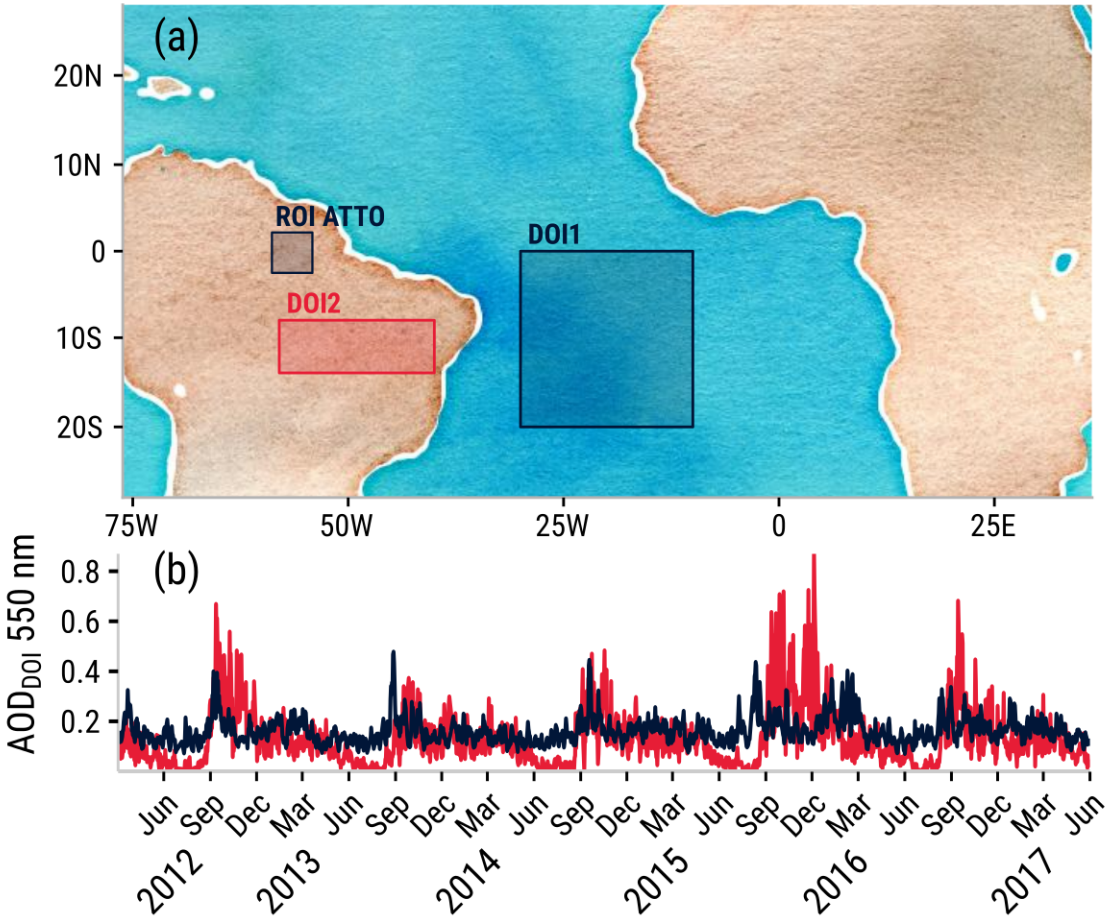

Figure 2. Aerosol optical depth (550 nm) observations in two different domains of interest shown in (a): DOI1 (Boundaries: 30W; 20S; 10W; 0S) and DOI2 (Boundaries: 58W; 14S; 40W; 8S). Time series of area-averaged AOD are shown in (b) for DOI1 (dark blue) and DOI2 (red). As a reference, the ATTO region of interest (ROI ATTO) is shown as a black rectangle in (a).

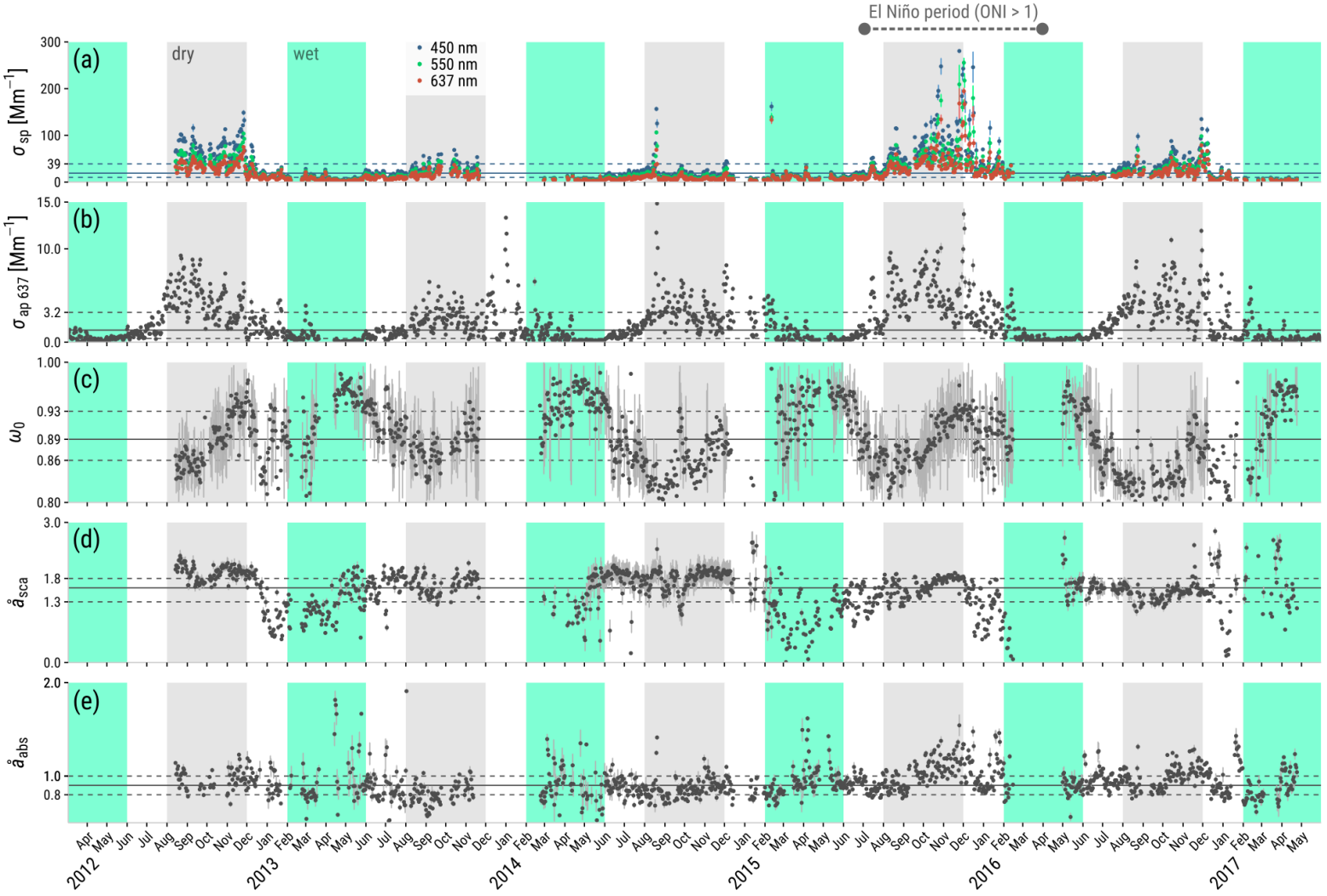

Figure 3. Overview of aerosol optical properties during the measurement period. (a) Scattering coefficient, (b) absorption coefficient at 637 nm, (c) single scattering albedo at 637 nm, (d) scattering Ångström exponent, and (e) absorption Ångström exponent. All data were averaged on 24-h intervals and standard errors are presented as vertical gray bars. Green and gray shaded areas correspond to the wet and dry seasons, respectively. First and third quartiles are represented as horizontal dashed lines, and medians as horizontal solid lines.

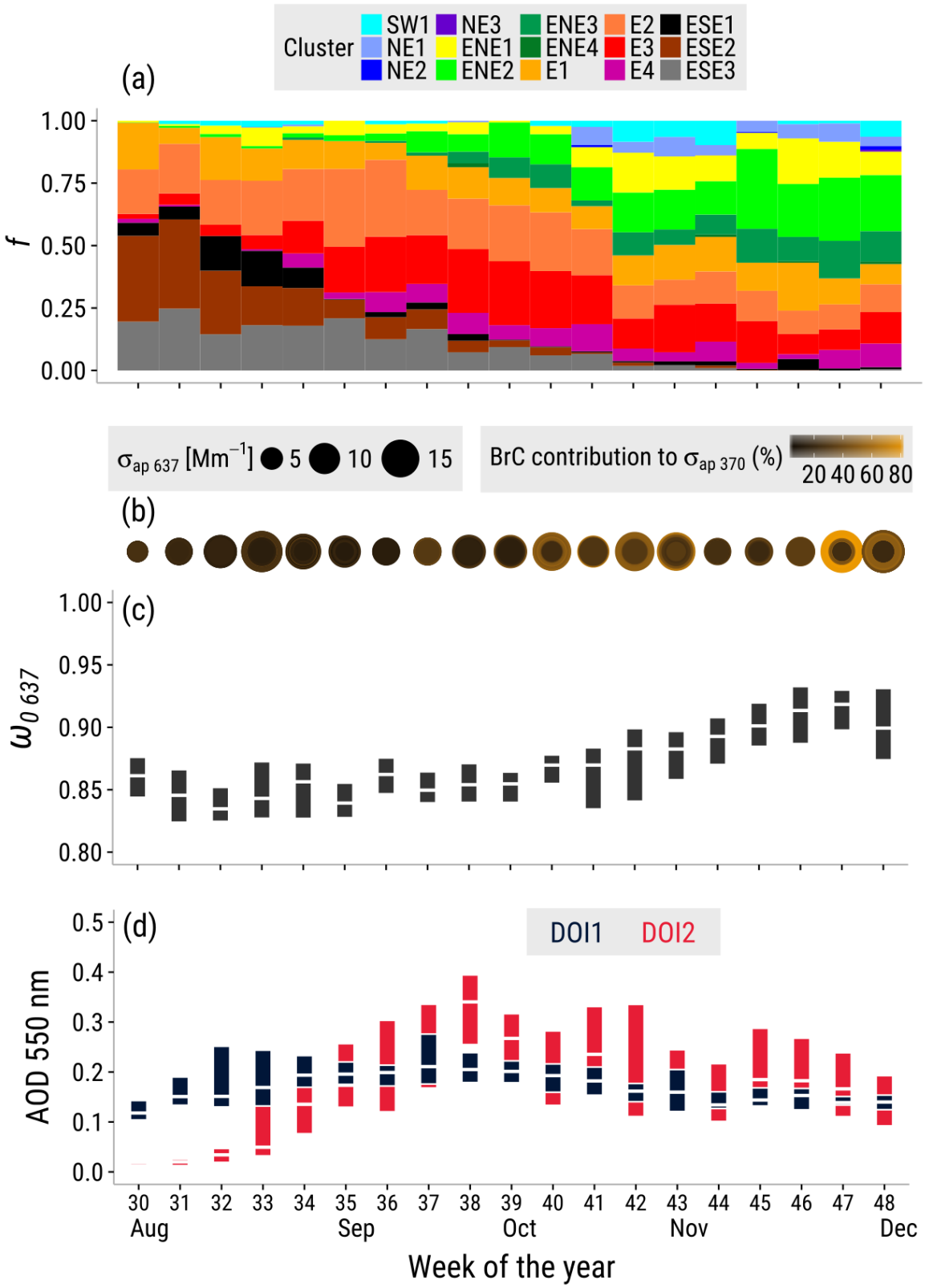

Figure 4. Multi-year (2012 – 2017) dry season weekly averages of (a) frequency of occurrence of BT clusters, *f*, (b) absorption coefficients at 637 nm, $\sigma_{ap\ 637}$, shown as circles with increasing diameters, the color scale corresponds to the relative BrC contribution to $\sigma_{ap\ 370}$, (c) single scattering albedo at 637 nm, $\omega_{0\ 637}$, and (d) aerosol optical depth at 550 nm (AOD) for the different domains of interest, DOI1 and DOI2, which cover regions of the South Atlantic Ocean and the southern Amazon, respectively. Boxplots in (c) and (d) represent the median (white segment) and the 25th and 75th percentiles (lower and upper box edges, respectively).

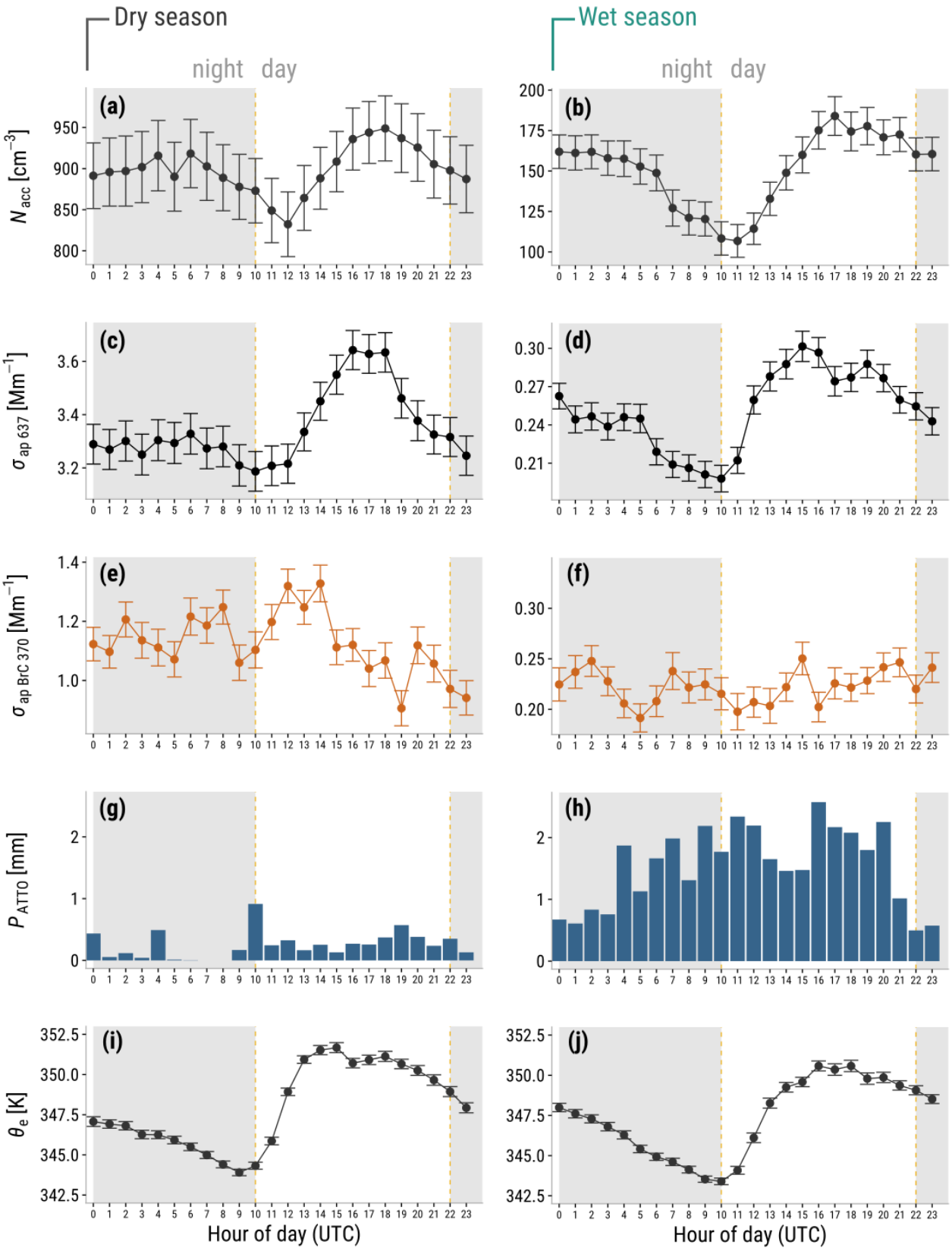

Figure 5. Diel variation of (a, b) median of the accumulation mode particle number concentration, N_{acc}, (c, d) median of the absorption coefficient at 637 nm, (e, f) median of the BrC absorption coefficient at 370 nm, (g, h) precipitation rate, and (i, j) median of the equivalent potential temperature. Gray and white backgrounds correspond to the night and day times, respectively. Error bars correspond to the standard error. Please note the different *y*-axis scales.

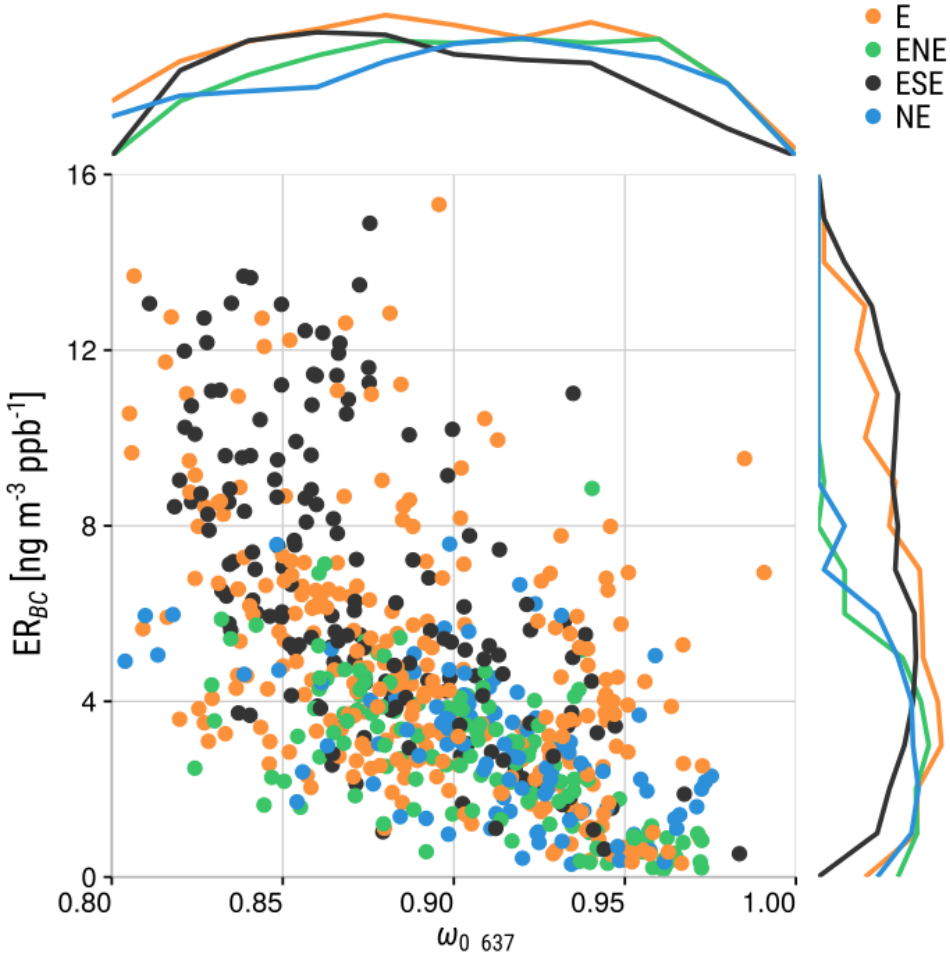

Figure 6. Sca /s. single scattering alb nts in log-scale) for

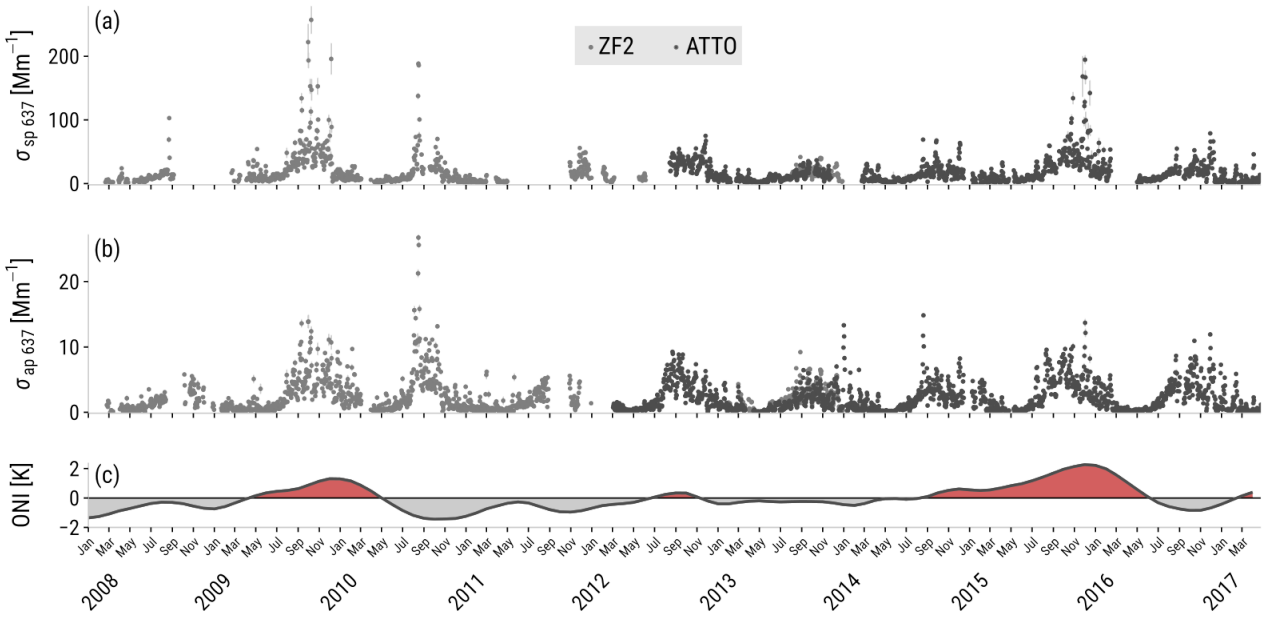

Figure 7. Scattering (a) and absorption (b) coefficient (637 nm) time series measured at the ZF2 and the ATTO sites from 2008 to 2016 (24-h averaged data). Increased scattering and absorption coefficients were observed under the influence of El Niño. (c) High ONI indicates active ENSO periods, shown as red shaded areas.

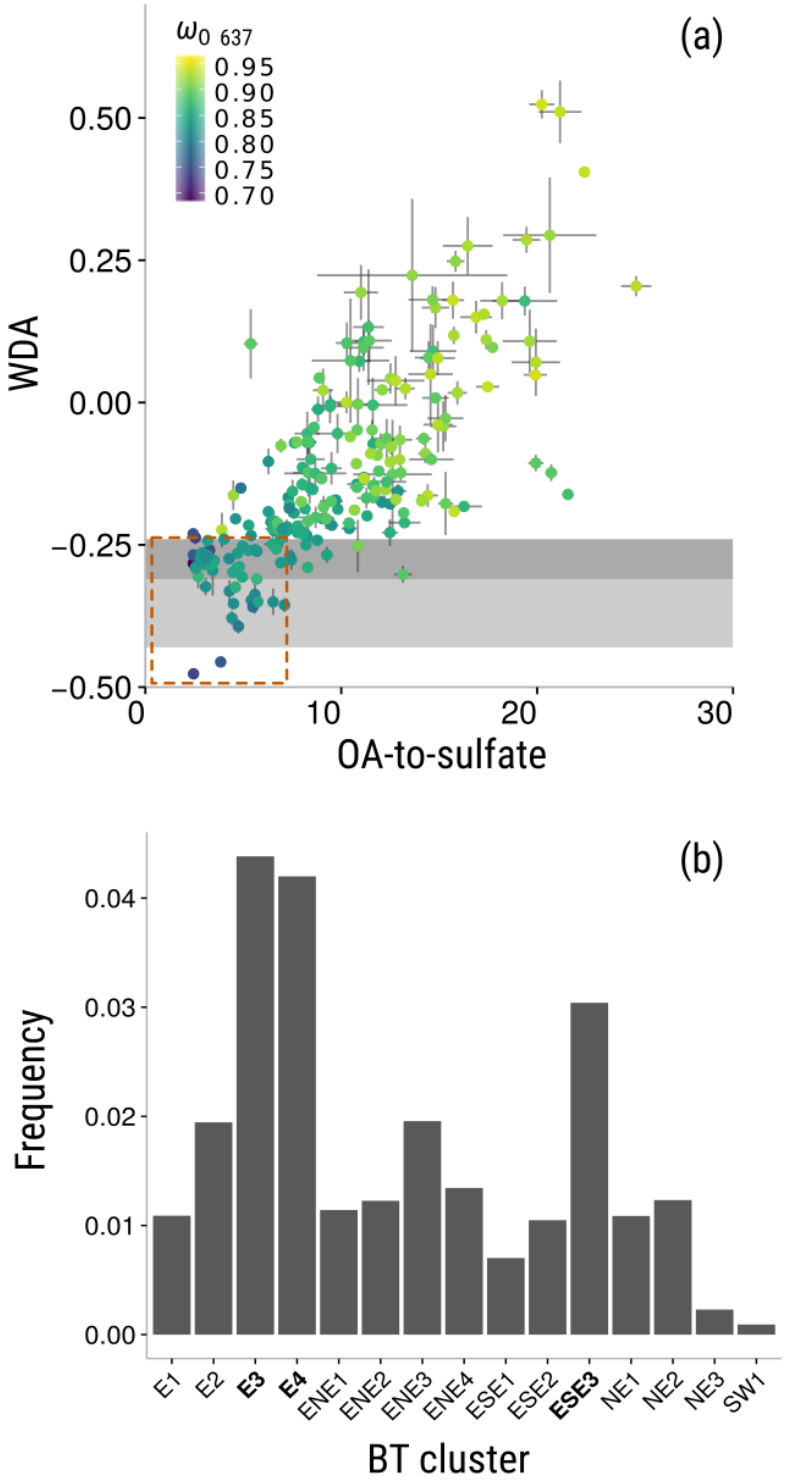

Figure 8. (a) Absorption wavelength dependence (WDA) as function of the OA-to-sulfate mass ratio during high-absorption periods in the dry season. The color scale indicates the ω_0 at 637nm. Gray shaded areas correspond to theoretical WDA for internally mixed BC (light gray), and externally mixed BC (dark gray). The data inside the dashed rectangle in (a) is used in (b) to identify the BT clusters that are more likely to bring BC to the ATTO site.

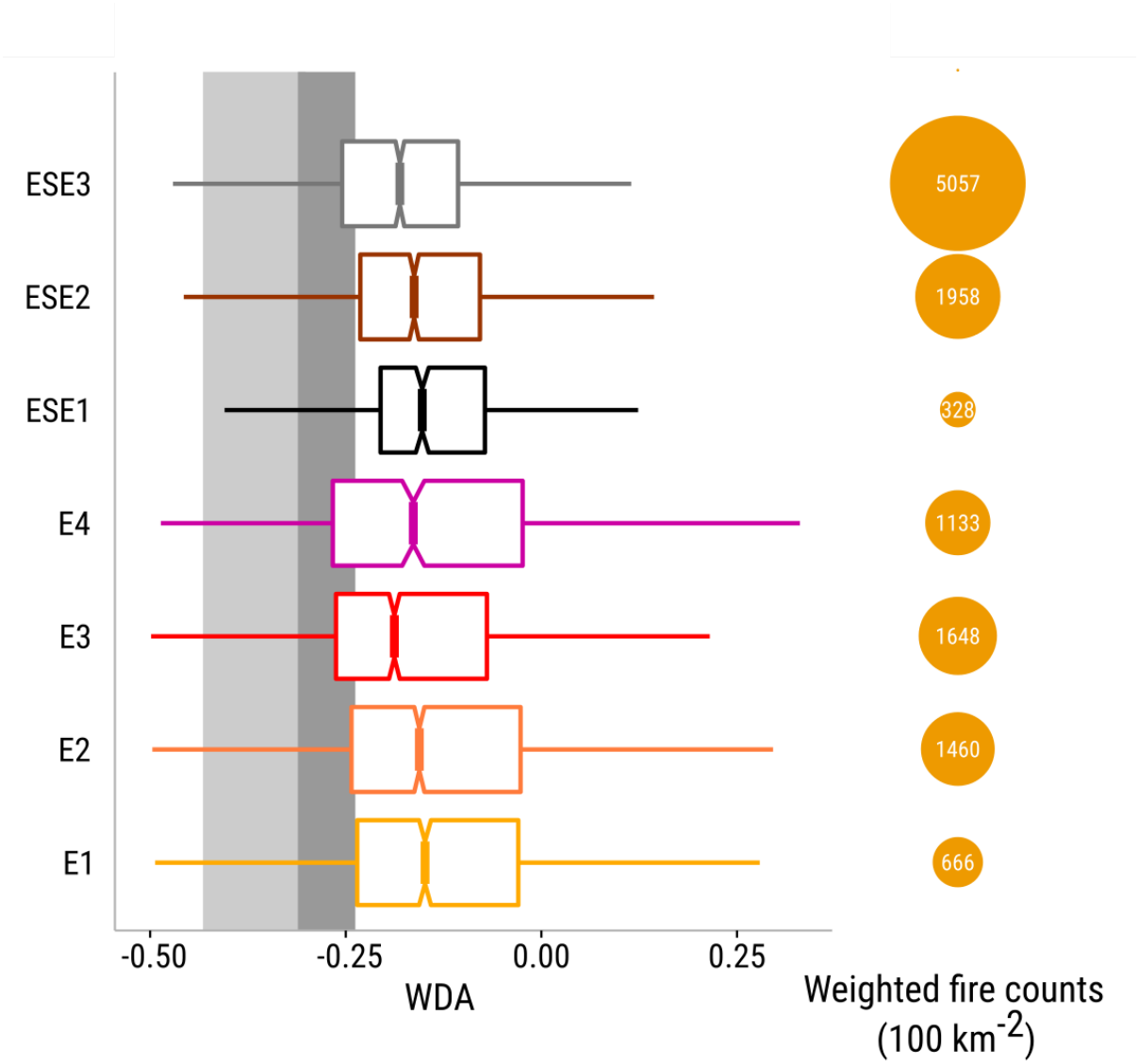

Figure 9. Wavelength dependence of $å_{abs}$ (WDA) for different trajectories in the dry season presented as box and whisker plots (left). The light and dark gray shaded areas correspond to the pure BC and internally mixed BC regimes, respectively. Notches correspond to 1.58 IQR $n^{-½}$. If notch ranges do not overlap, the medians are statistically different (95% confidence). The trajectory weighted fire counts for each BT cluster are shown as circles on the right side. The data presented here correspond to 1-h averages.

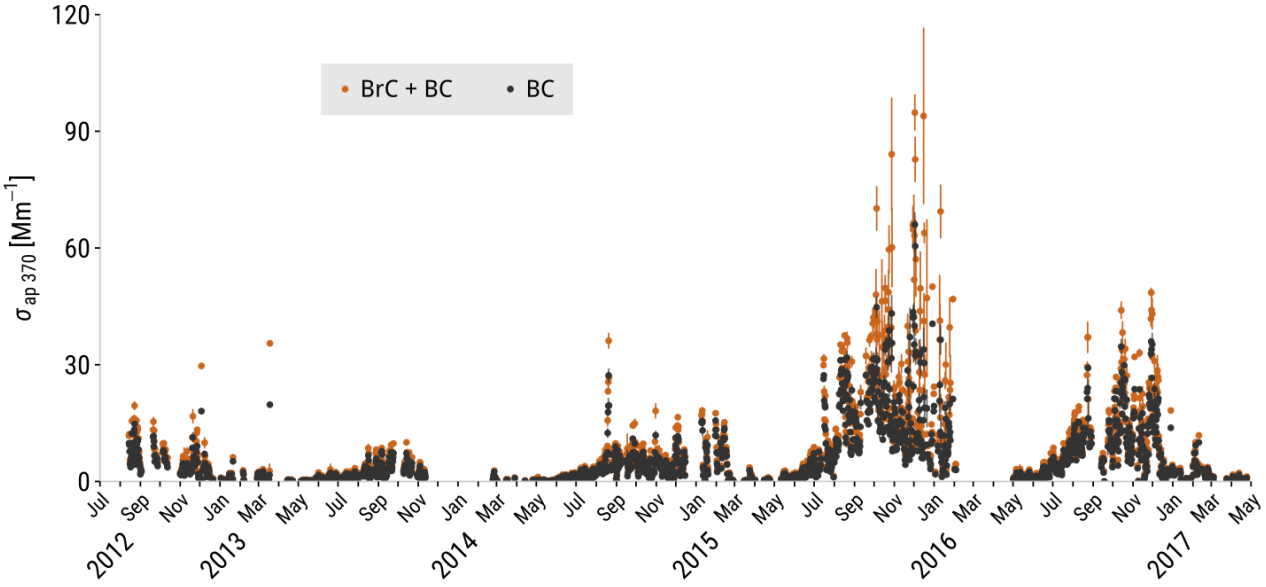

Figure 10. Total absorption at 370 nm (12-h average data) segregated by BC only (gray points) and BrC + BC (brown points). Error bars are equivalent to ± 1 standard error. Long-range transport dust events have been excluded from the analysis.

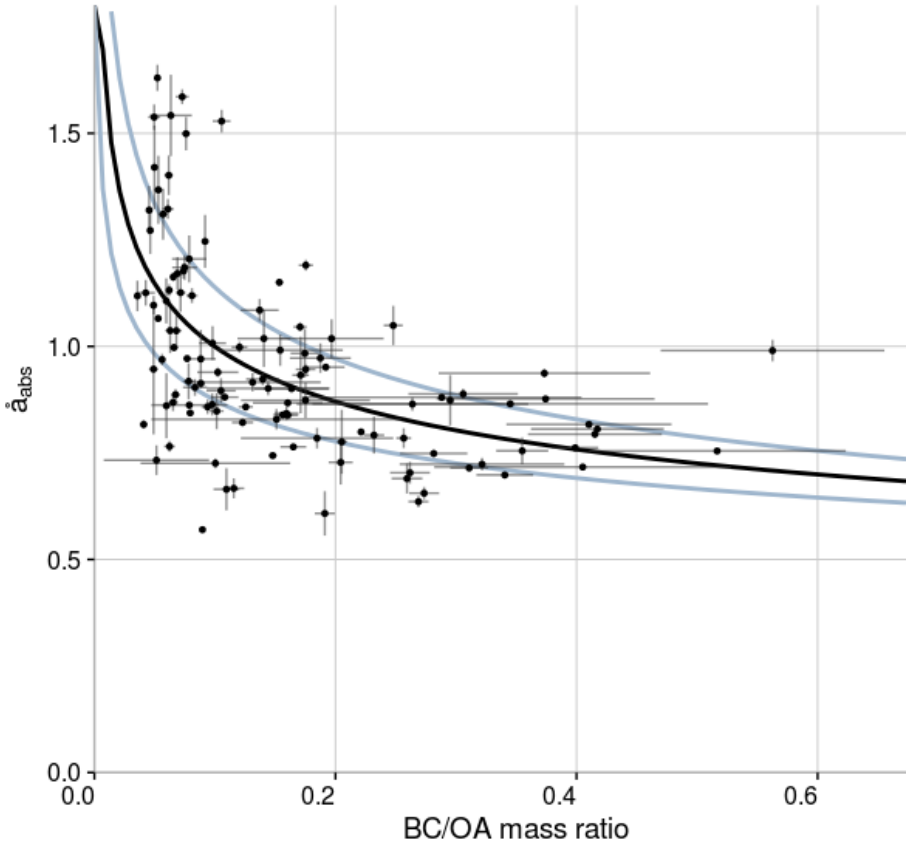

Figure 11. Absorption Ångström exponent ($å_{abs}$) as a function of the BC/OA mass ratio for selected dust events in the wet season. The black line corresponds to a non-linear least squares fit applied to the data ($y = x^{-0.199} \times 0.632$). The light blue lines correspond to the standard error of the fit.